

Published in final edited form as:

Nat Cardiovasc Res. ; 1(12): 1156–1173. doi:10.1038/s44161-022-00172-z.

Tyrosine-protein kinase Yes controls endothelial junctional plasticity and barrier integrity by regulating VE-cadherin phosphorylation and endocytosis

Yi Jin¹, Yindi Ding¹, Mark Richards¹, Mika Kaakinen², Wolfgang Giese^{3,4}, Elisabeth Baumann^{3,5}, Anna Szymborska^{3,4}, André Rosa^{3,4,13}, Sofia Nordling¹, Lilian Schimmel⁶, Emir Bora Akmeriç^{3,5}, Andreia Pena⁷, Emmanuel Nwadozi¹, Maria Jamalpour⁸, Katrin Holstein⁹, Miguel Sáinz-Jaspeado¹, Miguel O. Bernabeu^{10,11}, Michael Welsh⁸, Emma Gordon⁶, Claudio A. Franco^{7,12}, Dietmar Vestweber⁹, Lauri Eklund², Holger Gerhardt^{3,4,5}, Lena Claesson-Welsh¹

¹Department of Immunology, Genetics and Pathology, Uppsala University, Rudbeck, Beijer and SciLifeLab Laboratory, Uppsala, Sweden

²Oulu Centre for Cell-Matrix Research, Faculty of Biochemistry and Molecular Medicine, Biocenter Oulu, University of Oulu, Oulu, Finland

³Max Delbrück Center for Molecular Medicine, Berlin, Germany

⁴DZHK (German Centre for Cardiovascular Research), partner site Berlin, Germany

⁵Charité – Universitätsmedizin Berlin, Berlin, Germany

⁶Institute for Molecular Bioscience, Division of Cell and Developmental Biology, The University of Queensland, Brisbane QLD, Australia

⁷Instituto de Medicina Molecular - Joao lobo Antunes, Faculdade de Medicina, Universidade de Lisboa, Portugal

⁸Department of Medical Cell Biology, Uppsala University, Uppsala, Sweden

⁹Department of Vascular Cell Biology, Max Planck Institute for Molecular Biomedicine, Münster, Germany

¹⁰Centre for Medical Informatics, Usher Institute, The University of Edinburgh, UK

¹¹The Bayes Centre, The University of Edinburgh, UK

Correspondence to: Yi Jin; Lena Claesson-Welsh.

Correspondence should be addressed to: Lena Claesson-Welsh, at the address above or lena.welsh@igp.uu.se, and Yi Jin, at the address above or yi.jin@igp.uu.se.

¹³Current address: Molecular Medicine and Gene Therapy, Lund Stem Cell Centre, Lund University, BMC A12, 221 84 Lund, Sweden

Author Contributions Statement

Y.J. designed the study, performed experiments and analyzed data. Y.D., M.R., M.K., A.S., L.S., E.B.A., A.P., E.N., M.J., M.S.J. performed experiments, collected and analyzed data. W.G., E.B., A.R. analyzed imaging data. S.N. analyzed sc-RNA sequencing data. K.H. characterized antibody specificity. M.O.B., M.W., E.G., C.A.F., D.V., L.E., H.G. contributed to data analysis and interpretation. L.C.W. conceived, directed and financed the study. Y.J. and L.C.W. wrote the manuscript with input from all authors.

Competing Interest Statement

The authors declare no competing interests.

¹²Universidade Católica Portuguesa, Católica Medical School, Católica Biomedical Research Centre, Portugal

Abstract

Vascular endothelial (VE)-cadherin in endothelial adherens junctions is an essential component of the vascular barrier, critical for tissue homeostasis and implicated in diseases such as cancer and retinopathies. Inhibitors of Src cytoplasmic tyrosine kinase have been applied to suppress VE-cadherin tyrosine phosphorylation and prevent excessive leakage, edema and high interstitial pressure. Here we show that the Src-related Yes tyrosine kinase, rather than Src, is localized at endothelial cell (EC) junctions where it becomes activated in a flow-dependent manner. EC-specific *Yes1* deletion suppresses VE-cadherin phosphorylation and arrests VE-cadherin at EC junctions. This is accompanied by loss of EC collective migration and exaggerated agonist-induced macromolecular leakage. Overexpression of *Yes1* causes ectopic VE-cadherin phosphorylation, while vascular leakage is unaffected. In contrast, in EC-specific Src-deficiency, VE-cadherin internalization is maintained, and leakage is suppressed. In conclusion, Yes-mediated phosphorylation regulates constitutive VE-cadherin turnover, thereby maintaining endothelial junction plasticity and vascular integrity.

Endothelial cell-cell adhesions form an integral part of the vascular barrier, restricting the passage of molecules and cells across the vessel wall¹. The barrier in most organs is flexible, allowing remodeling of the embryonic and postnatal vascular beds and exchange of small molecules and fluid to maintain adult tissue homeostasis². During acute inflammation and in a range of chronic diseases, the barrier is weakened, leading to extravasation of blood constituents, promoting inflammation and progression of pathologies such as retinopathies and cancer¹⁻³. The maintenance of junctions and barrier function relies on junctional complexes consisting of cell-adhesion molecules formed between adjacent endothelial cells (ECs). Tight junctions limit vascular leakage preferentially in the central nervous system (CNS) and in arteries and post-arterial capillaries in peripheral tissues⁴⁻⁶. Adherens junctions, formed by vascular endothelial (VE)-cadherin and associated catenins, are crucial for regulating venous and capillary vascular permeability, leukocyte extravasation and collective cell migration⁷⁻¹³. VE-cadherin is rapidly internalized in response to inflammatory cytokines and vascular endothelial growth factor A (VEGFA), allowing transient opening of gaps at EC contacts¹. Although tyrosine phosphorylation of VE-cadherin has been implicated in the regulation of its internalization, the mechanisms of gap formation and vascular leakage have remained poorly understood^{14,15}. This is important, as exaggerated vascular leakage and the formation of edema are drivers of disease¹.

Three main tyrosine phosphorylation sites have been identified in VE-cadherin, Y658, Y685 and Y731^{16, 17}. Both Y658 and Y685 are phosphorylated in veins, but not in arteries, as a consequence of flow-induced activation of Src cytoplasmic tyrosine kinases¹⁸. Phosphorylated (p)Y658 relieves tension across VE-cadherin bridges through binding of the polarity protein LGN (leucine-glycine-asparagine repeat), which displaces VE-cadherin-associated p120 catenin¹⁹. Phosphorylation of Y685 is induced by flow as well as by inflammatory cytokines and VEGFA^{17, 18, 20}. Vascular leakage requires phosphorylation of Y685, as inferred from a Y685-to-phenylalanine (F) exchange mutant mouse, which

shows suppressed extravasation of large molecular weight tracers or cells in agonist-treated healthy tissues and in disease models^{11, 21, 22}. Leakage is accompanied by VE-cadherin endocytosis and reduced levels of pVE-cadherin¹⁸. Y731 is constitutively phosphorylated and its dephosphorylation by Src homology phosphatase 2 (SHP2) is a prerequisite for leukocyte extravasation^{11, 23}. Several additional phosphotyrosine phosphatases (PTPs), such as VE-PTP and density enhanced phosphatase 1 (DEP1; also denoted CD148), have been implicated in the regulation of VE-cadherin phosphorylation^{24, 25, 26}.

Src-mediated VE-cadherin phosphorylation on Y685 in response to VEGFA stimulation has been regarded as an important step in VEGFA-induced leakage^{11, 17, 19}. However, EC-specific *Src*-deficiency interferes with cell-matrix adhesion rather than cell-cell adhesion^{27, 28}. In addition to Src, ECs express the highly related cytoplasmic tyrosine kinases Yes and Fyn, the roles of which have remained poorly understood. *In vitro* studies have suggested distinct roles for Src, Yes and Fyn in regulating EC behaviors, despite their well-conserved Src homology 2 (SH2), SH3 and kinase domains²⁹. Accordingly, constitutive global gene inactivation results in abolished VEGFA-induced vascular leakage in constitutive gene inactivated *Src*^{-/-} or *Yes1*^{-/-} mice but not in *Fyn*^{-/-} mice³⁰.

Here, we demonstrate a critical role for Yes in the phosphorylation of VE-cadherin at all main phosphorylation sites, Y658, Y685 and Y731. Loss of VE-cadherin phosphorylation suppresses its endocytosis and interferes with cell-cell adhesion, leading to abnormal barrier properties with blunted collective migration, excessive macromolecular leakage and suppressed leukocyte extravasation. Forced phosphorylation of VE-cadherin by *Yes1* overexpression does not affect agonist-induced leakage; thus, macromolecular leakage is not controlled solely by the extent of VE-cadherin phosphorylation. In contrast, in *Src* deficiency, VE-cadherin endocytosis is unaffected, and vascular leakage is reduced. Therefore, Yes and Src differentially regulate VE-cadherin turnover, adherens junction stability and vascular leakage. We conclude that the two highly related cytoplasmic kinases have distinct and even opposing roles in the vasculature.

Results

Yes regulates shear stress-induction of pVE-cadherin

We investigated the pattern of VE-cadherin phosphorylation (pVE-cadherin) at Y685 in an intact vascular network (whole-mounted developing mouse retina at postnatal day 6; P6) in relation to the relative shear stress level. The specificity of the pY685 antibody was validated in VE-cadherin tyrosine to phenylalanine, Y685F, mutant mice (Extended Data Fig. 1a). A similar strategy was used to validate the specificity of another pVE-cadherin antibody against pY731 (Extended Data Fig. 1b-c). Shear stress in different regions of the retina vasculature was estimated using computational flow simulation on the PolNet platform³¹ (Fig. 1a, b), which models flow based on the vascular plexus geometry and the rheological properties of blood. The retinal vasculature was segmented into 5 regions: sprouting front (region 1); vein (2); capillaries near vein (3); capillaries near artery (4); artery (5) (Fig. 1b). Simulation showed that shear stress was the lowest at the sprouting front, correlating to a very low pVE-cadherin signal. In veins and capillaries (regions 2-4), with low-medium shear stress levels, the pVE-cadherin signal was markedly induced. In the artery, with very high

shear stress, the pVE-cadherin signal returned to low levels (Fig. 1b), in accordance with findings in organs such as the diaphragm, the bladder and the yolk sac^{18, 32}.

A similar pattern was seen *in vitro*; exposure of human umbilical vein endothelial cells (HUVECs) to low shear stress (3 dyn/cm²) induced pY685 VE-cadherin levels, whereas at high shear stress (20 dyn/cm²), VE-cadherin was unphosphorylated (Fig. 1c, d). The appearance of pVE-cadherin in HUVECs correlated with phosphorylation of Src family kinases (SFKs) at Y418, indicative of SFK activity, which was induced under low shear stress and suppressed under high shear stress (Fig. 1e-g). A direct relationship between Src activation and phosphorylation of VE-cadherin has been suggested¹⁷, however, the amino acid sequence around Y418 in the kinase domain of Src is identical in multiple SFKs. Yes, another SFK expressed by ECs, was preferentially localized to EC junctions, while Src displayed a weak junctional signal but abundant cytoplasmic and nuclear distribution (Fig. 1h). Moreover, *YES1* transcript levels were higher than *SRC* levels in HUVECs (7.8±0.5-fold; Figure 1i). The expression of both Src and Yes was further upregulated by low shear stress (Fig. 1e).

To compare the roles of Yes and Src in the regulation of VE-cadherin phosphorylation, *YES1*- or *SRC*-silenced HUVECs were subjected to 3 dyn/cm² shear stress. Silencing of either *YES1* (*siYES1*) or *SRC* (*siSRC*) did not affect the expression of the other (Extended Data Fig. 1d, e). However, *siYES1* strongly suppressed (82%) flow-induced phosphorylation of VE-cadherin at Y685 and Y658 (Fig. 1j, k; Extended Data Fig. 1f, g), while *siSRC* resulted in a partial loss (58%) of pY685 levels (Fig. 1j, k). Treatment of HUVECs exposed to 3 dyn/cm² flow with *siYES1* moreover suppressed flow induction of the pY418SFK signal, while treatment with *siSRC* was without effect (Fig. 1l, m), indicating that Yes but not Src, phosphorylates VE-cadherin at low shear stress. Single cell RNA sequence analysis of P6 and P10 retinal ECs showed overall higher expression of *Yes1* than *Src* *in vivo*, however, the expression of both was relatively uniform between non-proliferative vessel subtypes (Extended Data Fig. 1h, i; Supplementary table 1), while expression of VE-cadherin trended towards higher levels in arteries (Extended Data Fig. 1j). Combined, these data suggest that the different levels of VE-cadherin phosphorylation in arteries and veins (Fig. 1a, b) are not caused by different expression levels of *Yes1*, but by different extents of flow-induced Yes kinase activity.

VE-cadherin phosphorylation on Y658, Y685, and Y731 by Yes

A conditional, *Cdh5CreER^{T2}*³³-controlled *Yes1* knockout mouse (*Yes1* iECKO; Extended Data Fig. 2a) was generated to eliminate endothelial expression of *Yes1*. The deletion efficiency with tamoxifen treatment was 70% (Extended Data Fig. 2b). In the *Yes1* iECKO P6 retina, phosphorylation of VE-cadherin was downregulated by 74±15%, 78±10% and 72±23% at Y658, Y685 and Y731, respectively, compared to littermate controls (Fig. 2a-f; see Extended Data Fig. 1a-c for pY685 and pY731 antibody specificity; the pY658 antibody has been described¹⁸). In EC-specific *Src* knockout (*Src* iECKO; 80% deletion efficiency²⁸) pVE-cadherin levels decreased by 49±15% (Y658), 39±6% (Y685) and 46±7% (Y731) in the P6 retina (Fig. 2g-i, Extended Data Fig. 2c-e). In *Yes1* iECKO mice, pVE-cadherin levels were dramatically reduced in large veins, such as the *vena cava* (Extended Data Fig.

2f, g). Moreover, losing only one allele of *Yes1* in ECs led to 60% decrease in pY658 and pY685 VE-cadherin levels in P6 *Yes^{w/fl}:Cre⁺* retinas (Extended Data Fig. 2h, i). The long-term effect of endothelial Yes deficiency was examined in P22 mice, treated with tamoxifen at P1-3. The loss in VE-cadherin phosphorylation seen at P6 was still evident 3 weeks after recombination (Extended Data Fig. 2j, k), thus, other SFKs did not compensate for *Yes1* deficiency during this time period.

To study the cell autonomous function of *Yes1*, the *Rosa26R-YFP* reporter was introduced into the *Yes1* iECKO mouse line. One dose of tamoxifen at P3 generated chimeric recombination, labelling most, but not all, of the *Yes1*-deficient ECs with YFP. The YFP+ retinal ECs showed 45±12% lower pY685 VE-cadherin levels than adjacent YFP-ECs (Fig. 2j, k), indicating that Yes controls VE-cadherin phosphorylation in a cell-autonomous manner. The relatively limited reduction on pY685 VE-cadherin levels was expected since expression of the YFP reporter does not completely correlate with the *Yes1* gene deletion.

VE-cadherin is a substrate for the EC-specific phosphotyrosine phosphatase VE-PTP (*PTPRB*)^{24, 34}. Silencing of *PTPRB* in HUVECs markedly increased pY685 VE-cadherin levels (Extended Data Fig. 3a-c). Treatment of HUVECs with *siYES1* suppressed pY685 levels also in *PTPRB*-deficient ECs, indicating that Yes acts directly on VE-cadherin, rather than indirectly, by modulating VE-PTP activity.

Next, an inducible “floxed-STOP” *Yes1* overexpression mouse (denoted *Yes1* iECO) was generated by insertion of the mouse *Yes1* cDNA with an upstream floxed transcriptional stop signal into the *Hipp11* (*H11*) locus, controlled by the CAG promoter (Extended Data Fig. 4a). Following crossing with the *Cdh5CreER^{T2}* mouse line and treatment with tamoxifen, EC-specific *Yes1* overexpression was achieved. The overexpressed Yes protein localized to endothelial junctions in the retinas of *Yes1* iECO mice (Extended Data Fig. 4b), accompanied by a strong increase in the pY685 VE-cadherin signal. Strikingly, the pY685 VE-cadherin levels were increased at the sprouting front as well as in arteries in *Yes1* iECO P6 retinas to levels comparable to those in veins and capillaries (Fig. 2l, m). In mice with chimeric induction of *Yes1* overexpression, pVE-cadherin levels increased several-fold also in retinal capillaries and veins where levels were already high in the control (Fig. 2n, o). This indicates that in wildtype (WT) mice, pVE-cadherin levels relative to total VE-cadherin protein is limited. Thus, assuming that VE-cadherin in the *Yes1* iECO mouse is fully phosphorylated, less than 35% of the total VE-cadherin pool was phosphorylated in veins and capillaries in the WT. We conclude that the limiting factor in flow-regulated VE-cadherin phosphorylation is the expression level of Yes, which when sufficiently high, allows its activation and phosphorylation of VE-cadherin also under conditions of high shear stress such as in arteries. Interestingly, in the chimeric *Yes1* iECO mouse retina, branch points on both veins and arteries were more likely to be occupied by *Yes1* OE cells (Extended Data Fig. 4c, d), suggesting that ECs with high pVE-cadherin may be more resilient to disturbed flow at vessel bifurcations (note WSS changes at vessel branch points in Fig. 1a, rightmost panel). Alternatively, *Yes1* OE cells may be blunted in their ability to move away from bifurcations.

To compare the effects of Yes and Src overexpression on pY685 VE-cadherin, Src and Yes were introduced in HUVECs via lentiviral transduction. Forced overexpression of Src and Yes promoted increased pY685 VE-cadherin levels to a similar extent (Extended Data Fig. 5a-e). However, in Src overexpressing cells, both Src and pY685 VE-cadherin were detected in the cytoplasm, concentrated in the perinuclear region, while in Yes overexpressing cells, both Yes and pY685 were detected at broad folds at endothelial junctions (Extended Data Fig. 5a, compare pY685 VE-cadherin immunostaining in Yes and Src overexpressing cells). These results suggest that Yes is the main kinase regulating VE-cadherin phosphorylation at EC junctions.

Yes1 controls endothelial collective cell migration

The plasticity of endothelial cell-cell adhesions is known to impact collective cell migration³⁵. During vascular development, ECs migrate from veins towards arteries³⁶. To explore whether Yes-mediated VE-cadherin phosphorylation impacts endothelial vein to artery migration, the dual reporter-Cre, iSuRe-Cre, was exploited for EC tracing³⁷. In the iSuRe-Cre model, MbTomato-reporter expression is genetically linked with deletion of the target gene. The localization of MbTomato-labelled ECs in control and *Yes1* iECKO retinas was determined at P7 and P15 after partial recombination induced at P3 (Fig. 3a). Artery and vein regions were segmented and the localization of MbTomato+ ECs was mapped in a 2D, shown with the relative distance between veins and arteries on the x-axis (vein: 0.0; artery: 1.0) and the distance from optic nerve to sprouting front on the y-axis (Fig. 3b). At P7, the vein-to-artery distribution of MbTomato+ ECs in *Yes1* iECKO retinas was similar to the control (Fig. 3c-e). However, in the radial distribution, MbTomato+ ECs in *Yes1* iECKO retinas were positioned closer to the optic nerve, compared to control MbTomato+ ECs (Fig. 3c, f, g). At P15, MbTomato+ ECs in *Yes1* iECKO retinas were significantly more concentrated to arteries with only scarce presence in veins and capillaries (Fig. 3c-e). Moreover, at P15, *Yes1* iECKO MbTomato+ ECs were localized closer to the optic nerve than in the control (Fig. 3c, f, g). With a higher degree of recombination following multiple tamoxifen injections at P1, 3, 6, and 9, the concentration of Yes-deficient ECs in arteries was striking (Fig. 3h and i), accompanied by widening of the artery diameter in the distal region, away from the optic nerve (Fig. 3i, j). Thus, compared to WT ECs, Yes-deficient ECs are privileged to migrate towards arteries in the developing retina. In retinas with chimeric deletion of VE-cadherin, certain arteries were entirely devoid of VE-cadherin-expressing ECs (Extended Data Fig. 6a), in agreement with the finding that loss of pVE-cadherin-dependent cell-cell adhesion promoted migration towards arteries³⁸.

A monolayer scratch assay was employed to investigate how Yes-deficiency affects EC migration *in vitro*. Individual cells from the first three rows from the migratory front were tracked and grouped by their initial position (Extended Data Fig. 6b; Supplementary video 1). Control ECs in the different rows migrated collectively at a similar speed, while by silencing *YES1*, cells in rows 1-3 separated from neighbouring cells and migrated at a faster speed (Extended Data Fig. 6c) and *YES1*-silenced cells from the first and second rows migrated further than the control cells (Extended Data Fig. 6d). Next, the activities of the well-known regulatory factors for migration, Rho-GTPases CDC42, Rac1 and RhoA were examined (Extended Data Fig. 6e-h). The basal activity of CDC42 was increased in *YES1*-

silenced cells. Basal RhoA activity showed the same trend, while Rac1 was unaffected, indicated that perturbed activity of small GTPases contributed to EC dysregulation in *Yes1* deficiency^{39, 40}.

The loss of *YES*-dependent VE-cadherin phosphorylation and endothelial migration did however not interfere with sprouting angiogenesis. In *Yes1* iECKO mice, retinal vascular outgrowth at P6 was normal compared to Cre+ control mice (*Yes1*^{wt/wt}, *Cdh5CreER*^{T2+}) (Extended Data Fig. 7a,b), and the number of filopodia on tip cells at the sprouting front was unaffected (Extended Data Fig. 7c,d). Retinal vascular outgrowth was unaffected also in mice carrying a Y685F VE-cadherin mutation (Extended Data Fig. 7e, f). In contrast, VE-cadherin null mice (*Cdh5* iECKO) exhibited a strong hypersprouting phenotype paralleled by delayed outgrowth (Extended Data Fig. 7g, h). Thus, the lack of VE-cadherin tyrosine phosphorylation in the *Yes1* iECKO mouse does not result in a null phenotype. The retinal vascular area was significantly reduced also in *Yes1* iECO mice compared to control (*H11-Yes1* 0/0, *Cdh5CreER*^{T2+}) (Extended Data Fig. 7i, j). Therefore, VE-cadherin is strictly required, but its phosphorylation is dispensable for normal sprouting angiogenesis. Moreover, excessive phosphorylation of VE-cadherin is accompanied by disturbed vascular development.

We further investigated whether the lack of VE-cadherin phosphorylation would affect other cellular processes involved in angiogenesis. VEGFA induced angiogenic sprouting from aortic rings from both control and *Yes1* iECKO mice (Extended Data Fig. 8a, b), but *Yes1* iECKO sprouts were longer (Extended Data Fig. 8c), in accordance with enhanced cell motility. EC proliferation in developing retinas was assessed by EdU incorporation followed by immunostaining of the endothelial-specific nuclear protein ERG. The fraction of proliferative ECs was not changed in *Yes1* iECKO mice compared to the control (*Yes1*^{fl/fl}, *Cdh5CreER*^{T2-}) (Extended Data Fig. 8d, e). Moreover, deleting *Yes1* in ECs did not affect the number of Cleaved Caspase3-positive apoptotic cells in postnatal retinas, (Extended Data Fig. 8f, g). These data show that *Yes*-deficiency impacts collective EC migration while sprouting, proliferation and apoptosis still proceed.

Adherens junction morphology in *Yes*- and *Src*-deficiency

EC adaptation to microenvironmental demands for remodelling, perfusion or permeability is dependent on dynamic changes at adherens junctions, which appear with linear or jagged morphologies⁴¹ (Fig. 4a). In the WT P6 retina, VE-cadherin in arterial ECs formed linear junctions, while jagged junctions appeared only on veins and capillaries exhibiting phosphorylated VE-cadherin (Extended Data Fig. 9). *Yes1* silencing did not prevent formation of jagged junctions but the response to shear stress (3dyn/cm²) was lower than in the control cells (Fig. 4b, c). In contrast, silencing of *SRC* in HUVECs exhibited a strong inhibitory effect on jagged junctions both in static and flow conditions (Fig. 4b, c). In P6 retinas, the appearance of jagged junctions in the veins of both *Yes1* and *Src* iECKO mice was suppressed but more extensively so in the *Src* iECKO condition (Fig. 4d, e). These data show that changes in VE-cadherin morphology from linear to jagged does not directly correlate with its phosphorylation status.

VE-cadherin internalization requires Yes, but not Src

In the *siYes1*-treated, flow-exposed HUVECs, VE-cadherin appeared in broad clusters along the junctions (Fig. 4b). The nature of these clusters was further explored by live cell imaging of HUVECs expressing GFP-tagged VE-cadherin. In control cells, VE-cadherin was detected in junction-proximal endocytic vesicles, which moved away from the junction. The internalized VE-cadherin vesicles disappeared within 2-5 minutes (Fig. 5a, upper panels; Supplementary video 2). In *Yes1*-silenced HUVECs, VE-cadherin instead formed large clusters, which existed for 15-30 minutes before gradually disappearing, to be replaced by new clusters (Fig. 5a, middle panels; Supplementary video 3). In *SRC*-silenced HUVECs, VE-cadherin endocytic vesicles were observed with similar dynamics as in control cells (Fig. 5a, lower panels; Supplementary video 4).

These data indicated that VE-cadherin internalization was affected by Yes-deficiency. VE-cadherin internalization was followed by an antibody feeding assay. Constitutive internalization of VE-cadherin was efficiently inhibited by *Yes1* silencing, whereas *SRC* silencing had no effect (Fig. 5b, c). HUVECs cultured under flow (3 dyn/cm²) showed increased VE-cadherin internalization, blocked by *siYes1* but not *siSRC* treatment (Fig. 5d; Extended Data Fig. 10a). Additionally, VEGFA-induced VE-cadherin internalization was arrested by *siYes1* but not *siSRC* (Fig. 5e; Extended Data Fig. 10b). VE-cadherin endocytic vesicles enriched in pY685 VE-cadherin were detected *in vivo*, just below the plasma membrane, in *vena cava* ECs from control mice. The prevalence of endocytotic vesicles was markedly reduced in the *Yes1* iECKO *vena cava* (Fig. 5f, g). Combined, these results indicate that phosphorylation of VE-cadherin is strictly required for its constitutive internalization, which is a prerequisite for junctional plasticity.

p120 catenin has been implicated in the regulation of VE-cadherin endocytosis as binding of p120 masks an internalization motif in VE-cadherin¹⁴. The presence of the p120 catenin/VE-cadherin complex was assessed by coimmunoprecipitation, which showed similar levels under basal conditions and a trend towards increased complex formation in VEGFA-treated *siControl* and *siYes1* HUVECs (Extended Data Fig. 10c, d). Thus, complex formation with p120 was unaffected by loss of VE-cadherin tyrosine phosphorylation.

Ultrastructure of Yes-deficient endothelial junctions

The decreased VE-cadherin internalization in Yes-deficient ECs could potentially impact junction organization, which was addressed by transmission electron microscopy (TEM) analysis of the mouse ear dermis subjected or not to intradermal injection of VEGFA. In *Yes1* iECKO mice, the electron dense junctional area expected to mark high actin density, known to be disrupted in conjunction with vascular leakage^{1, 42, 43}, was smaller than that in control mice under basal conditions (Fig. 6a, c). While the electron dense area decreased upon VEGFA injection in WT mice, it increased in the *Yes1* iECKO condition (Fig. 6a, c), suggesting disturbed junctional dynamics under *Yes1*-deficiency. The electrondense cortical actin area in *Src* iECKO mice was similar to control mice with a trend towards decreased area with VEGFA-treatment (Fig. 6b, d).

In agreement, live imaging of cells labelled with fluorescent actin revealed that actin stress fibres were misaligned and moved towards the periphery in *Yes1*- but not in Control- or *SRC*-silenced HUVECs (Supplementary videos 5-8). Moreover, VEGFA treatment significantly increased the relative abundance of cortical actin in *Yes1*-silenced HUVECs but not in *SRC*-silenced or control cultures. In the *siSRC* cultures, there was instead an increased proportion of stress fibers relative to cortical actin (Fig. 6e, f) in agreement with the different ultrastructural TEM morphologies of *Yes1* iECKO and *Src* iECKO vessels.

Increased vascular permeability in *Yes1* iECKO mice

The consequence of *Yes*-deficiency for vascular barrier function was addressed using several *in vivo* methods. The basal level of vascular permeability was tested by tail-vein injection of Evans blue followed by a 2-hour circulation period. Increased levels of Evans blue in the interstitial tissue of the ear skin were detected in *Yes1* iECKO mice (Extended Data Fig. 11a). Blood-brain barrier integrity, assessed by the leakage of Evans blue and cadaverine into the cerebral tissue, was unaffected by *Yes1*-deficiency (Extended Data Fig. 11b, c). Thus, the vascular barrier was compromised in the *Yes*-deficient dermis and potentially other tissues but not in the CNS.

The permeability of developing retinal vessels was studied by cardiac injection of fixable fluorescent tracer (dextran-TRITC, 10 kDa) in P6 mice. Leakage of the tracer into the perivascular tissue was observed preferentially at the vascular sprouting front, possibly marking an immature vascular barrier, and neither *Yes1*-deletion nor overexpression changed the number of leakage sites at the sprouting front (Fig. 7a, b). However, an increased frequency of venous leakage was observed in *Yes1* iECKO retinas (8 leakage sites observed in 11 veins from 10 retinas) in comparison to the control retinas (2 leakage sites in 14 veins from 9 retinas) (Fig. 7a, c). In contrast, leakage from veins was not elevated in *Yes1* iECEO retinas (Fig. 7c).

Permeability of the mature vasculature was investigated by intravital confocal imaging of adult dermal vessels. In the WT dermis, pVE-cadherin was detected in some but not all venous vessels and, unexpectedly, in some arterioles (Extended Data Fig. 11d). This is in contrast to the pattern observed in the retina, where veins but not arteries display pVE-cadherin signals. The detection of pVE-cadherin in dermal arterioles may reflect flow patterns that do not conform to the expected high flow-low phosphorylation pattern, or alternatively, higher expression levels of VE-cadherin. Nevertheless, VE-cadherin phosphorylation in dermal vessels was markedly reduced in adult *Yes1* iECKO mice (Extended Data Fig. 11d, e), similar to the findings in the developing retina. To monitor leakage, a fluorescent tracer was injected into the tail vein, and leakage from dermal vessels in the ear was monitored after local injection of VEGFA (Fig. 7d, Supplementary video 9, 10). Leakage was initiated at individual sites in venules and capillaries in both control and *Yes1* iECKO mice (Fig. 7e, Supplementary video 11, 12). Quantification of leakage sites/vessel length showed that the leakage site density was increased in both venules and capillaries in *Yes1* iECKO mice (Fig. 7f). The fluorescence intensity profile at leakage sites demonstrated that leakage appeared sooner after VEGFA-injection in *Yes1* iECKO mice and that leakage was more vigorous in the absence of *Yes1* compared to the WT (Fig.

7g). The number of leakage sites was unaffected in *Yes1* iECHO mice compared to WT mice (Fig. 7h), indicating that leakage is not directly regulated by VE-cadherin tyrosine phosphorylation. In contrast to the increased leakage observed in *Yes1* deficiency, *Src* iECHO mice exhibited a reduced number of leakage sites after VEGFA injection (Fig. 7i). The kinetics of the remaining leakage sites was unaffected (Fig. 7j). These results show that while *Yes* is required for restricting formation of leakage sites at junctions, *Src* is required for such sites to form.

The Y731 phosphosite in VE-cadherin is required for leukocyte extravasation. Leukocyte populations were analysed by FACS in fluids collected by peritoneal lavage in mice 24 h after saline or VEGFA was injected. In agreement with the phenotype of Y731F mice¹¹, monocyte (CD11b+ LY6G-) extravasation was reduced in VEGFA-treated *Yes1* iECHO mice compared to the control (Fig. 7k).

Combined, these results show that loss of *Yes*-mediated phosphorylation of VE-cadherin results in dysregulation of endothelial junctions with increased leakage of macromolecules but suppressed extravasation of inflammatory cells.

Discussion

Regulation of endothelial junctions has been ascribed to *Src*^{44, 45}. The viral form, v-*Src*, localizes to adherens junctions⁴⁶, and gap junction-dependent cell-cell communication is regulated by c-*Src*⁴⁷. Although broad screens for *Src* kinase substrates have revealed hundreds of candidate molecules⁴⁸, only a handful have been validated including p85-Cortactin, p110-AFAP1, p130Cas, p125FAK and p120-catenin²⁷. A common denominator for several of these *Src* substrates is the involvement in actin-dependent processes. In agreement, EC-specific loss of *Src* expression results in impaired cell-matrix adhesion properties²⁸.

Even less is known about *Yes* substrates. *Yes* phosphorylates the tight junction component occludin in epithelial and endothelial cells (ECs)⁴⁹, but the functional consequence is unclear. *Yes* has been implicated in negative regulation of the cell cycle by phosphorylating cyclin-dependent kinase 4⁵⁰. *Yes* moreover plays a role in T-lymphocyte immunity by phosphorylating CD46⁵¹ and Collapsin Response Mediator Protein 2 (CRMP2)⁵². However, using an *in vitro* kinase-based screen to identify substrates for SFKs, no specific substrate for *Yes* was identified⁵³. The important role of *Yes* in EC cell-cell adhesion is suggested by its abundant junctional localization; single-cell transcriptomics shows that *Yes1* is more abundant in ECs than in other cell types in a range of mouse tissues (<https://tabula-muris.ds.czbiohub.org/>)⁵⁴.

An important conclusion is that the different SFKs must be targeted individually as they serve different, sometimes opposing purposes. *Yes*-deficiency resulted in loss of VE-cadherin phosphorylation, suppressed endocytosis, clustering of VE-cadherin and increased macromolecular leakage. In contrast, in *Src*-deficiency, VE-cadherin phosphorylation was reduced, albeit to a lesser extent, VE-cadherin internalization remained unaffected, and macromolecular leakage was suppressed. Combined, these data challenge the cause-

consequence relationship between VE-cadherin phosphorylation, internalization and the formation of junctional gaps and macromolecular leakage. Specifically, the loss of the Y685 site has been shown to prevent tracer leakage in healthy and pathological tissues^{11, 22, 55}. Furthermore, VEGFA- or histamine-induced acute vascular leakage in mature dermal vessels is established at pVE-cadherin-high sites in capillaries and postcapillary venules^{5, 56}. Combined, the data suggest that VE-cadherin phosphorylation is required for its constitutive endocytosis and it sensitizes ECs to rapid VEGFA-induced endocytosis and gap formation at EC junctions. Nevertheless, an additional trigger is required for gap formation and macromolecular leakage. Importantly, phosphorylation of VE-cadherin could also be a prerequisite for gap closure. Thus, the dysregulated leakage from Yes-deficient vessels may be a consequence of uncoordinated opening and closure of junctional gaps in addition to incomplete sealing in the resting state due to loss of plasticity, akin to a stiff rubber band that has lost its normal elasticity.

The mechanism underlying the distinct effects of Yes and Src on VE-cadherin may be related to their different subcellular localization, allowing phosphorylation of different subcellular pools of VE-cadherin, in addition to the potential involvement of other kinase-specific substrates. Src localizes to focal adhesions in freshly seeded ECs, where it phosphorylates p125FAK²⁷. Endothelial FAK-deficiency results in dismantling of adherens junctions⁵⁷, and VEGFA-induced vascular leakage requires FAK-induced phosphorylation of β -catenin⁵⁸, underscoring the important role of matrix adhesion in the regulation of EC junctions. The subcellular localization of cytoplasmic tyrosine kinases is influenced by NH2-terminal fatty acid modification. Both Yes and Src are myristoylated while Yes is in addition palmitoylated, potentially contributing to steer the subcellular localization and trafficking of Src and Yes^{59, 60}. Their different subcellular localization would also be compatible with the distinct regulation of the actin cytoskeleton by Yes and Src: Yes-, but not Src-deficient HUVECs exhibited an increase in cortical actin and loss of actin stress fibers. Moreover, the electron dense, cortical actin-enriched junctional area in Yes-deficient dermal vessels was low in the basal condition but increased markedly upon administration of VEGFA. The abnormal actin arrangements in the absence of Yes provide a potential mechanistic underpinning for the changes in junctional dynamics with formation of VE-cadherin clusters and the block in VE-cadherin internalization.

Binding of p120-catenin to a VE-cadherin juxtamembrane motif has been implicated in VE-cadherin stabilization¹⁴, and in agreement, dephosphorylation of VE-cadherin at Y658 increases the binding affinity for p120 *in vitro*^{19, 61}. The vascular barrier is normal in mice with a mutation of this endocytic motif in VE-cadherin, but the vessel density is decreased in the developing retina⁶². VE-cadherin/p120 complex-formation occurs however independently of VE-cadherin phosphorylation¹⁸. In accordance, p120/VE-cadherin complex formation occurred also in the absence of Yes. Importantly, in contrast to certain VE-cadherin endocytosis-deficient mutant models⁶², the expression levels of VE-cadherin and p120 were unaffected by *Yes1*-deletion. Moreover, YAP/TAZ signaling is implicated in EC adhesion and VE-cadherin internalization⁶³; the potential contribution of Yes to YAP/TAZ signaling warrants further studies.

The exaggerated macromolecular leakage in *Yes1*^{-/-} vessels is at odds with the leakage phenotype of Y685F mice, which show suppressed leakage of macromolecules^{11, 22} and suppressed reverse transmigration of neutrophils²¹. The difference in phenotypes between the Y685F- and *Yes*-deficient mouse models may be related to the fact that *Yes*-deficiency affects additional molecular regulators at endothelial junctions yet to be discovered. However, the block in monocyte extravasation is in agreement with the phenotype of the Y731F vasculature¹¹. Thus, although the phosphosites are similarly regulated by *Yes*, Y658, Y685 and Y731 serve distinct purposes by regulating the extravasation of either macromolecules or inflammatory cells through different mechanisms and potentially at geographically distinct sites in the vasculature.

The new insights presented here deepen the understanding of the complex regulation of adherens junctions, where an interplay between several cytoplasmic tyrosine kinases, such as *Yes* and *Src*, orchestrates the process when gaps form and close again and when the vascular surface becomes prepared to dock and expel inflammatory cells.

Methods

Mice

Yes1^{flox/flox} mouse strain was generated by flanking exon 3 with *loxP* sites, introduced by homologous recombination on the genetic C57Bl/6 background (Taconic/Cyagen; Extended Data Fig. 2a). The generation of *Src*^{flox/flox} and *Cdh5*^{flox/flox} strains has been described^{28, 55}. These strains were crossed with *Cdh5(PAC)-CreER^{T2}* mice (a kind gift from Dr. Ralf Adams) to generate endothelial-specific knockout of *Yes1*, *Src* or *Cdh5*. For analysis in mosaic knockout, the fluorescent reporter mouse line B6.129X1-Gt(ROSA)26Sor^{tm1(EYFP)Cos/J} (Stock Number 006148, The Jackson Laboratory) was introduced to indicate Cre activity with YFP expression. For retinal EC distribution analysis, the *iSuRe-Cre* mouse strain (a kind gift from Dr. Rui Benedito) was crossed with the *Yes1*^{flox/flox} mouse. *iSuRe-Cre+*; *Yes1*^{wt/wt}; *Cdh5CreER^{T2}+* mice were used as control for all analyses of the *iSuRe-Cre+*; *Yes1*^{fl/fl}; *Cdh5CreER^{T2}+* strain, to ensure that the observed phenotype was not due to Cre toxicity. Conditional *Yes1* knock-in mouse *H11-CAG-STOP-Yes1* was generated using CRISPR/CAS (Taconic/Cyagen; Extended Data Fig. 4a). The VE-Cad Y685F and the VE-Cad Y731F mice have been described¹¹. Both males and females were included in the experiments. Animal husbandry and procedures were in accordance with institutional guidelines and approved by the Institutional Review Board for animal experimentation at Uppsala University (Permit 5.8.18-06789/2018).

Intravital vascular leakage assay

Intravital imaging of the mouse ear dermis⁵ was performed following systemic administration of 2000-kDa dextran by tail-vein-injection. Mice were anaesthetised by intraperitoneal (i.p.) injection of ketamine-xylazine (120 mg/kg ketamine, 10 mg/kg xylazine) to a surgical level, and the ear was secured to a solid support. Mice were maintained at a body temperature of 37°C throughout the experiment for a maximum 90 minutes. Time-lapse imaging was performed using single-photon microscopy (Zeiss LSM 710) and a high N. A water-immersion lens (CF175 apochromat 25xW N.A1.1, Nikon).

For intradermal EC stimulation, a volume of 0.1 μL recombinant mouse VEGFA164 (Peprotech), 100 ng/ μL , was injected using a submicrometer capillary needle. 10 kDa TRITC Dextran was used as a tracer for VEGFA. Leakage sites were identified in time-lapse imaging following VEGFA injection as defined sites of concentrated dextran in the extravascular space. The researcher was blinded to the genotype of the mice when performing the analyses.

In vivo wall shear stress analysis

Flow simulation from the images of retinal vasculature shown by CD31 staining was performed using the PolNet platform³¹. Flat-mounted retinas were imaged at an area including one artery, one or two veins and the complete capillary network in between by tile scanning confocal microscopy (Leica SP8) using a 40X objective. 3D reconstruction of the vascular network was performed using maximum intensity projection of the vessels illustrated by CD31 immunostaining. A heat map of the relative shear stress level was generated based on the flow simulation by assigning an inlet at the artery and outlet at the vein. Regional average shear stress levels were obtained and plotted combined with the pVE-cadherin levels.

Retinal EC distribution analysis

Chimeric recombination was induced in iSuRe-Cre+ mice at P3 by i.p. injection of tamoxifen (100 $\mu\text{g}/\text{mouse}$, Sigma). Retinas were taken at P7 and P15, immunostained for CD31 and flat-mounted. Images were taken by z-stack tile scanning using a 10X objective on a confocal microscope (Leica SP8). Maximum intensity projection images of whole retinas were used for image segmentation, which was performed with ImageJ resources. The maximum projection of the MbTomato channel threshold was established to distinguish MbTomato+ cells from the background. Outliers with a radius between 0.2-1.0 μm were removed. The CD31 channel (after maximum projection) was used to define the outlines of veins and arteries; the optic nerve was used as a mask to define a referential system. For computational analysis, a bespoke Python-based workflow was employed, accessible on GitHub (<https://github.com/wgiese/retina-vein-artery-cs>). For every pixel in the image, three numbers were computed (using the mask as referential): (1) distance to the nearest vein (d_v), (2) distance to the nearest artery (d_a) and (3) radial distance to the optic nerve (r). From these measures, the relative distances by $\phi_{v-a} = d_v/(d_v + d_a)$ were obtained. The EC distribution was computed by performing the operation for all YFP-positive pixels, which were used as a proxy for EC distribution. A kernel density estimation was used to approximate the underlying EC distribution in the 2D coordinate system spanned by ϕ_{v-a} and r . High degree recombination was induced at P1, P3, P6 and P9 by i.p. injection of tamoxifen (100 $\mu\text{g}/\text{mouse}/\text{day}$, Sigma) and retinas were taken at P15 for analysis.

Retinal single cell RNA-sequencing data

Single cell RNA-sequencing data generated from WT P6 and P10 retinas⁶⁶ was obtained from the Sequence Read Archive (<https://www.ncbi.nlm.nih.gov/sra>), accession number SRP322112, and preprocessed with cellranger (v5.0.1) using the mm10 reference genome. ECs included in the analysis were defined as positive for *Pecam1*, *Cdh5*, *Kdr* expression or as having been characterized as ECs in the original publication. Raw counts were

normalized with a pooling size factor-based strategy as implemented in *scran* (v.1.18.7). Subtype annotations were generated using *scmap* (v.1.16.0) using the cluster assignment described in the original publication. Differential gene expression analysis was carried out using *MAST* as implemented in *Seurat* (v.4.1.1). The effects of dropouts in the data were reduced with imputation with the *magic* python package (v.0.1.1; $k = 9$, $ka = 3$, $t = 1$) and graphs were generated with *ggplot2* (v.3.3.6).

Vessel leakage in postnatal retina

Recombination was induced at P1-3 by i.p. injection of tamoxifen (100 µg/day/mouse, Sigma). At P6, mice were anesthetized, and 10 kDa TRITC-dextran-lysine (100 µg/g body weight, TdB Labs) was injected into the left heart ventricle. After 10 minutes, eyes were removed and fixed in 4% paraformaldehyde (PFA; Sigma) for 2 hours at room temperature (RT). A needle puncture on the cornea facilitated fast fixation. Retinas were immunostained with CD31 to visualize blood vessels. Images were acquired by z-stack tile scanning in a confocal microscope (Leica SP8). A site of leakage was scored positive if dextran was detected in the perivascular region.

Immune cell infiltration assay

Recombination was induced in 8- to 12-week-old mice by gavage with tamoxifen (2 mg/day/mouse, Sigma) for 5 consecutive days. After 2 days resting, saline or VEGFA (5 µg/kg body weight) was administered through i.p. injection. After 24 h, mice were sacrificed, 5 mL of PBS was injected intraperitoneally, and recruited cells were collected after abdominal palpation. Cells were immunostained with CD11b (101206, Biolegend) and LY6G (127608, Biolegend) antibodies for FACS analysis.

Transmission electron microscopy

Eight- to 12-week-old control or *Yes1* iECKO mice were treated with intradermal injection of VEGFA164 (10 ng, Peprotech) in the ear skin. The other ear served as an untreated control. Mice were anesthetized and perfused first with 10 mL Hank's balanced salt solution (HBSS) and then 12 mL cold fixative (1% glutaraldehyde (Sigma), 4% PFA in 0.1 M phosphate buffer) through the left ventricle. Ears were cut and placed in fixative for 30 min at 4°C, washed 3 times with PBS, dehydrated and embedded in Epon, LX112 (Ladd Research Industries). Imaging was performed with a Tecnai G2 Spirit 120 kV transmission electron microscope (Fei Europe) and Quamesa CCD camera. Image analysis was done with Fiji processing package of Image J2 software.

Aortic ring assay

Thoracic aortas were taken from P7 mice and cut into 1 mm rings after removal of the connective tissues. Rings were embedded between two layers of rat tail collagen, type I (Thermo Fisher Scientific), and cultivated in Dulbecco's modified Eagle's medium (DMEM) (Gibco) supplemented with 10% fetal bovine serum (FBS) and VEGFA (PeproTech, 30 ng/mL). 4-OH-tamoxifen (5 µg/mL, Sigma) was added to the culture for 48 hours to induce recombination. After 4 days of initial cultivation, samples were fixed in 4% PFA (Sigma) and analysed by microscopy after immunostaining.

Proliferation

EC proliferation was assessed by i.p. injection of 5-ethynyl-2'-deoxyuridine (EdU, 100 µg/mouse, Thermo Fisher Scientific) at P6. Mice were sacrificed 2 hours after injection, and retinas were removed and fixed in 4% PFA (Sigma). EdU staining of retinas was performed using the Click-iT EdU imaging kit (Thermo Fisher Scientific). The samples were costained with antibodies against ERG to identify EC nuclei. Images were taken by confocal microscopy (Leica SP8) and analyzed by ImageJ.

Isolation of mouse lung ECs

Mice were treated with tamoxifen (100 µg/day/mouse, Sigma) at P1-3. Lungs were taken at P6 and dissociated to obtain cell suspensions using the MACS dissociation kit (Miltenyi Biotec). Isolation of ECs from mouse lungs was performed using anti-CD31 antibody (BD Pharmingen)-conjugated Dynabeads (Thermo Fisher Scientific). RNA from the isolated ECs was extracted immediately by using an RNeasy mini plus kit (QIAGEN).

Cell culture

HUVECs (PromoCell) were cultured at 37°C, 5% CO₂ in MV2 medium with supplied supplements (PromoCell). Cells were tested for cell morphology and cell type-specific markers using flow cytometric analyses by the vendor. For VEGFA stimulation, confluent cells were starved in MV2, 0.2% FBS without supplements for 5 hours. The same medium with VEGFA165 (50 ng/mL, Peprotech) was added and cells incubated at 37°C for the indicated time periods.

Yes and Src overexpression *in vitro*

SRC cDNA was cloned into pLV-CMV-IRIS-PURO-mScarlet plasmid at restriction enzyme site XhoI using In-Fusion Cloning (Takara). *YES1* cDNA was cloned into the pLV-CMV-IRIS-PUR-mScarlet plasmid at XhoI site using In-Fusion Cloning (Takara). Lentivirus constructs of control-m-Scarlet, c-Src-mScarlet, and Yes-mScarlet were packaged into lentivirus in HEK-293T cells by co-transfection of third generation lentiviral packaging plasmids with PEI 2500 (BioScientific). Lentivirus containing supernatant was harvested on day 2 and 3 after transfection. Lentivirus was concentrated by Lenti-X concentrator (Clontech, 631232). Transduced target HUVECs were selected with puromycin (1 mg/mL) after 24 h and used for assays after 72 h.

Scratch wound healing assay

HUVECs were seeded at a density of 50,000 cells/well into a 96-well ImageLock™ tissue culture plate (Essen BioScience) and incubated in MV2 medium overnight followed by standardized scratching using WoundMaker™ (Essen BioScience). Cells were washed with PBS, and the plate was placed into an IncuCyte ZOOM (Essen BioScience) and scanned every 15 min for 12 h using a 10× objective, during which data were collected using ZOOM software (Essen BioScience). Cellular migration was analyzed using MTrackJ in ImageJ by manually marking the cells at each time frame. The migration speed of one cell was obtained by dividing the migration distance by time.

Confocal live cell imaging

HUVECs were seeded at full confluency on glass-bottom plates (MatTek) and cultured in MV2 medium overnight. Fresh medium with SiR-actin dye (Cytoskeleton) was added to the cells and incubated for two hours. The cell monolayer was scratched using a 2 μ L pipette tip and changed to fresh medium. The plates were then placed on a Leica SP8 microscope equipped with a humidified CO₂ incubator (Leica Microsystem). Time-lapse z-stack images were scanned every 1 min for 3 hours.

In vitro flow treatment

HUVECs were seeded at full confluency on μ -slides (Ibidi) coated with fibronectin (1 μ g/mL, Sigma) and cultured overnight in degassed MV2 medium. The slides were then connected to the Ibidi pump system to allow degassed medium to flow through at 3 or 20 dyn/cm² shear stress for 24 h at 37°C in a CO₂ incubator. Static control cells were cultured on slides in an incubator for the same time period. Cells were fixed in 1% PFA for 10 min for immunofluorescence or lysed in RIPA buffer (Thermo Fisher Scientific) for western blots.

VE-cadherin internalization assay

Control or *YES1*-silenced confluent HUVECs were incubated with an antibody against the VE-cadherin extracellular domain (Clone BV6, MABT134, Merck Millipore, 10 μ g/mL) at 4°C for 1 hour in MV2 basal medium containing 3% bovine serum albumin (BSA) (Sigma) without supplements. Unbound antibody was removed by rinsing cells in ice-cold MV2 basal medium. Cells were then cultured at 37°C for 4 hours in the presence of 150 μ M chloroquine (Sigma) in MV2 medium with supplements. For VE-cadherin internalization under flow, cells were first cultured under 3 dyn/cm² flow for 20 hours before adding the antibody (Clone BV6, MABT134, Merck Millipore, 10 μ g/mL) and chloroquine (150 μ M) in the medium followed by continued culturing under flow for 4 hours. Cells were then washed for 8 min with PBS containing 25 mM glycine and 3% BSA with Ca²⁺, Mg²⁺, pH 2.7, to remove the antibody from the cell surface followed by rinsing with PBS and fixation with 2% PFA for 10 min at RT. Total VE-cadherin was stained with an antibody generated in another species (AF1002, R&D Systems). Samples were mounted on slides with Fluoromount G (Southern Biotech) and analyzed by confocal imaging.

RNA interference

siRNAs targeting human *YES1*, *SRC* or *PTPRB* (Sigma) were transfected into HUVECs by using Lipofectamine RNAiMAX (Thermo Fisher Scientific). Control cells were transfected with control siRNA that did not target any specific gene. siRNAs were mixed with lipofectamine and added to the cells at a concentration of 10 nM and incubated overnight before changing to fresh medium. The cells were used for experiments 48 h after transfection. The knockdown efficiency was validated by quantitative PCR. *YES1* siRNA: SASI_Hs01_00086922; *SRC* siRNA: SASI_Hs01_00112907; *PTPRB* siRNA: EHU158501, Sigma; Control siRNA: MISSION siRNA universal negative control (SCI001).

Immunofluorescence

Mice were sacrificed, and tissues removed and fixed in 2% PFA (eyes and ears were fixed for 1 h, *vena cava* was fixed for 15 min). Samples were incubated in PBS, 0.5% Triton X-100, 1% BSA for 3 hours at RT and then with primary antibodies overnight at 4°C. After 3 washes at RT, samples were incubated with secondary antibodies overnight at 4°C, washed 3 times and mounted on slides for imaging. For staining of cultures, cells were fixed in 1% PFA for 10 min after treatment. After fixation, the cells were washed 3 times in PBS and permeabilized in PBS, 0.1% Triton X-100 for 5 minutes, followed by blocking in 1% BSA for 30 minutes and incubation with primary antibodies overnight at 4°C. Cells were washed 3 times in 0.1% Triton X-100, incubated with secondary antibodies for 1 hour at RT, washed 3 times and mounted. Imaging was done using Leica SP8 (Leica Microsystems) confocal microscopes with LAS X software (3.5.7.23225). Image processing and analysis were performed using ImageJ software.

Antibodies against pVE-cadherin Y685 or Y731 were generated by immunizing rabbits with phosphopeptides of the corresponding regions of mouse VE-cadherin (New England Peptide). The pY658 antibody was a kind gift from Dr Elisabetta Dejana, IFOM, Milano, Italy and Uppsala University, Sweden). The antibodies were purified and precleared by incubation on fixed and permeabilized *Cdh5* null mouse ECs before use. The commercial antibodies used were goat anti-mouse VE-cadherin (AF1002, R&D Systems, 1:500), mouse anti-VE-cadherin-alexa-647 (561567, Becton Dickinson, 1:500) goat anti-mouse CD31 (AF3628, R&D Systems, 1:500), chicken anti-GFP (ab13970, Abcam, 1:1000), rabbit anti-ERG (ab92513, Abcam, 1:500), mouse anti-Yes (610376, BD Biosciences, 1:400), mouse anti-Src (Clone GD11, Merck Millipore, 1:400), and Alexa Fluor 647-phalloidin (A-22287, Thermo Fisher Scientific, 1:100). Secondary antibodies conjugated with Alexa Fluor dyes were obtained from Thermo Fisher Scientific or Jackson ImmunoResearch Laboratories.

Quantitative PCR

RNA was extracted and purified using RNeasy Plus kit (Qiagen). RNA concentrations were measured by a Nanodrop spectrophotometer (Thermo Fisher Scientific) and adjusted to equal concentrations, followed by reverse transcription using SuperScript III (Thermo Fisher Scientific). Real-time quantitative PCR was performed on a Bio-Rad real-time PCR machine using SsoAdvanced qPCR reagent (Bio-Rad). The housekeeping gene ribosomal protein L19 (*Rpl19*) was used as an internal control. The comparative Ct method was used to calculate fold differences.

Primer sequences were as follows: mouse *Yes1*: forward: 5'-AGTCCAGCCATAAAATACACACC-3', reverse: 5'-TGATGCTCCCTTTGTGGAAGA-3'; mouse *Rpl19*: forward: 5'-GGTGACCTGGATGAGAAGGA-3', reverse: 5'-TTCAGCTTGTGGATGTGCTC-3'; human *YES1*: forward: 5'-CTCAGGGGTAACGCCTTTTGG-3', reverse: 5'-CACCACCTGTAAACCAGCAG-3'; human *SRC*: forward: 5'-GACAGGCTACATCCCCAGC-3', reverse: 5'-CGTCTGGTGATCTTGCCAAA-3'; human *RPL19*: forward: 5'-TCGCTCTAGTGTCTCCG-3', reverse: 5'-GCGGGCCAAGGTGTTTTTC-3';

human *PTPRB*: forward: 5' - GCGGACCAGGATTCCCTCTA-3', reverse: 5' - AACTCCCGGATGGTCC-3'.

Rho-GTPase activity assay

Control or *YES1*-silenced HUVECs were starved at 37°C in basal MV2 medium with 0.2% FBS for 3 hours and stimulated with VEGFA164 (50 ng/mL, PeproTech) for 15 minutes. The activities of the Rho GTPases Rac1, CDC42 and RhoA were detected using kits from Cytoskeleton. Briefly, 300 µg of freshly prepared cell lysates were incubated with Rhotekin-RBD (RhoA) or PAK-PBD (CDC42, Rac1) beads for 1 hour, 4°C. Beads were washed 5 times and boiled in Laemmli buffer with β-mercaptoethanol. Samples were separated by SDS-PAGE (4-12% gradient gel) (Thermo Fisher Scientific), and blotting was performed to detect Rac1, CDC42 and RhoA with antibodies supplied in the kit.

Immunoprecipitation

Control or *YES1*-silenced HUVECs were starved at 37°C in basal MV2 medium with 0.2% FBS for 3 hours and stimulated with VEGFA164 (50 ng/mL, PeproTech) for 15 minutes followed by lysis in 50 mM Tris-HCl pH 7.5, 5 mM EDTA, 150 mM NaCl, 0.5% NP-40) supplemented with protease and phosphatase inhibitor cocktails (Roche). Lysates (300 µg) were incubated with 1.5 µg VE-cadherin antibody (AF1002, R&D Systems) overnight at 4°C. Protein G Sepharose beads (Cytiva) were incubated for 3 hours at 4°C. Beads were washed 5 times with lysis buffer, and proteins denatured and released from beads by boiling in β-mercaptoethanol-containing Laemmli buffer.

Western blot

Proteins were separated by SDS-PAGE (4-12% gradient gel) (Thermo Fisher Scientific), transferred to nitrocellulose membranes (GE Healthcare), and incubated sequentially with primary and horseradish peroxidase (HRP)-conjugated secondary antibodies. Signals were detected using enhanced chemiluminescence (Cytiva) and images retrieved using BioRad ChemiDocMP and analyzed using Image Lab software. The following primary antibodies were used: rabbit anti-VE-cadherin Y685 (CP1981, ECM Biosciences, 1:1000); goat anti-mouse VE-cadherin (AF1002, R&D Systems, 1:1000); rabbit anti-pSrc (Y418) (44-660G, Thermo Fisher Scientific, 1:1000); mouse anti-Yes (610376, BD Biosciences, 1:1000); and mouse anti-p120-Catenin (610133, BD Biosciences, 1:1000); Mouse anti-c-Src (05-184, Millipore, 1:1000), Rabbit anti-GAPDH (2118, Cell signaling, 1:5000) The secondary antibodies used were horseradish peroxidase (HRP)-conjugated anti-rabbit IgG (NA934, Cytiva), HRP-conjugated anti-mouse IgG (NA931, Cytiva), and HRP-conjugated anti-goat IgG (P0449, Dako). Secondary antibodies were used at a dilution of 1:7500.

Statistics and Reproducibility

Statistical analysis was performed using GraphPad Prism software. Statistical significance in comparisons between two groups was determined by two-tailed Student's t-test or Welch's t-test. Two-way ANOVA was used to compare between groups in time course experiments. Variances were similar between the groups compared. Differences were considered significant at $P < 0.05$. For animal experiments, no statistical methods were used

for predetermine sample sizes. The experiments were not randomized. The investigators were not blinded to allocation during the experiment and outcome assessment.

Supplementary Material

Refer to Web version on PubMed Central for supplementary material.

Acknowledgements

We gratefully acknowledge Elisabetta Dejana (Uppsala University; IFOM Milano) and Fabrizio Osenigo (IFOM, Milano) for the pY658-VE-cadherin antibody. Euro-BioImaging ERIC and Biocenter Oulu Electron Microscopy core facility supported by University of Oulu and Biocenter Finland are acknowledged for providing infrastructure allowing ultrastructural analyses. We gratefully acknowledge Dr. Alexandre Dubrac, Université de Montreal, Canada, for providing annotations for the single cell RNA-sequencing data of retinas, Dr. Rui Benedito, Centro Nacional de Investigaciones Cardiovasculares (CNIC), Madrid, Spain, for providing the iSuRe-Cre mouse model and Dr. Ralf Adams, Max-Planck Institute, Münster, Germany for providing the *Cdh5(PAC)-CreER^{T2}* mice. This study was supported by the Swedish Research Council (2020-01349), the Knut and Alice Wallenberg foundation (KAW 2020.0057 and KAW 2019.0276), Fondation Leducq Transatlantic Network of Excellence Grant in Neurovascular Disease (17 CVD 03) to LCW, HG, CAF and MB, Fundagao para a Ciencia e Tecnologia (PTDC/MED-PAT/31639/2017; CEECIND/04251/2017), European Research Council (679368): CAF, Deutsche Forschungsgemeinschaft (KFO342, P2; CRC1450, B03) to DV, the Academy of Finland (LE380986) and the Sigrid Jusélius Foundation to LE. The processing of the single cell RNA-sequencing data was enabled by resources in project SNIC 2021/22-221 provided by the Swedish National Infrastructure for Computing (SNIC) at UPPMAX, partially funded by the Swedish Research Council through grant agreement no. 2018-05973.

Data Availability

Full source data for retinal EC distribution analysis is available on Zenodo. Single cell RNA-sequencing data generated from WT P6 and P10 retinas⁶⁶ was obtained from the Sequence Read Archive (<https://www.ncbi.nlm.nih.gov/sra>), accession number SRP322112. Additional data supporting the findings in this study are included in the main article and associated files. Source data are provided with this paper.

Code Availability

Analysis code for retinal EC distribution can be accessed via: <https://github.com/wgiese/retina-vein-artery-cs>

References

1. Claesson-Welsh L, Dejana E, McDonald DM. Permeability of the Endothelial Barrier: Identifying and Reconciling Controversies. *Trends Mol Med.* 2021; 27: 314–331. [PubMed: 33309601]
2. Komarova YA, Kruse K, Mehta D, Malik AB. Protein Interactions at Endothelial Junctions and Signaling Mechanisms Regulating Endothelial Permeability. *Circ Res.* 2017; 120: 179–206. [PubMed: 28057793]
3. Wettschureck N, Strlic B, Offermanns S. Passing the Vascular Barrier: Endothelial Signaling Processes Controlling Extravasation. *Physiol Rev.* 2019; 99: 1467–1525. [PubMed: 31140373]
4. Nitta T, et al. Size-selective loosening of the blood-brain barrier in claudin-5-deficient mice. *J Cell Biol.* 2003; 161: 653–660. [PubMed: 12743111]
5. Honkura N, et al. Intravital imaging-based analysis tools for vessel identification and assessment of concurrent dynamic vascular events. *Nat Commun.* 2018; 9: 2746. [PubMed: 30013228]
6. Richards M, et al. Claudin5 protects the peripheral endothelial barrier in an organ and vessel-type-specific manner. *Elife.* 2022; 11

7. Corada M, et al. Vascular endothelial-cadherin is an important determinant of microvascular integrity in vivo. *Proc Natl Acad Sci U S A*. 1999; 96: 9815–9820. [PubMed: 10449777]
8. Allingham MJ, van Buul JD, Burridge K. ICAM-1-mediated, Src- and Pyk2-dependent vascular endothelial cadherin tyrosine phosphorylation is required for leukocyte transendothelial migration. *J Immunol*. 2007; 179: 4053–4064. [PubMed: 17785844]
9. Turowski P, et al. Phosphorylation of vascular endothelial cadherin controls lymphocyte emigration. *J Cell Sci*. 2008; 121: 29–37. [PubMed: 18096689]
10. Schulte D, et al. Stabilizing the VE-cadherin-catenin complex blocks leukocyte extravasation and vascular permeability. *EMBO J*. 2011; 30: 4157–4170. [PubMed: 21857650]
11. Wessel F, et al. Leukocyte extravasation and vascular permeability are each controlled in vivo by different tyrosine residues of VE-cadherin. *Nat Immunol*. 2014; 15: 223–230. [PubMed: 24487320]
12. Hayer A, et al. Engulfed cadherin fingers are polarized junctional structures between collectively migrating endothelial cells. *Nat Cell Biol*. 2016; 18: 1311–1323. [PubMed: 27842057]
13. Cao J, et al. Polarized actin and VE-cadherin dynamics regulate junctional remodelling and cell migration during sprouting angiogenesis. *Nat Commun*. 2017; 8: 2210. [PubMed: 29263363]
14. Nanes BA, et al. p120-catenin binding masks an endocytic signal conserved in classical cadherins. *J Cell Biol*. 2012; 199: 365–380. [PubMed: 23071156]
15. Adam AP. Regulation of Endothelial Adherens Junctions by Tyrosine Phosphorylation. *Mediators Inflamm*. 2015; 2015 272858 [PubMed: 26556953]
16. Potter MD, Barbero S, Cheresh DA. Tyrosine phosphorylation of VE-cadherin prevents binding of p120- and beta-catenin and maintains the cellular mesenchymal state. *J Biol Chem*. 2005; 280: 31906–31912. [PubMed: 16027153]
17. Wallez Y, et al. Src kinase phosphorylates vascular endothelial-cadherin in response to vascular endothelial growth factor: identification of tyrosine 685 as the unique target site. *Oncogene*. 2007; 26: 1067–1077. [PubMed: 16909109]
18. Orsenigo F, et al. Phosphorylation of VE-cadherin is modulated by haemodynamic forces and contributes to the regulation of vascular permeability in vivo. *Nat Commun*. 2012; 3: 1208. [PubMed: 23169049]
19. Conway DE, et al. VE-Cadherin Phosphorylation Regulates Endothelial Fluid Shear Stress Responses through the Polarity Protein LGN. *Curr Biol*. 2017; 27: 2727. [PubMed: 28898639]
20. Li X, et al. VEGFR2 pY949 signalling regulates adherens junction integrity and metastatic spread. *Nat Commun*. 2016; 7 11017 [PubMed: 27005951]
21. Owen-Woods C, et al. Local microvascular leakage promotes trafficking of activated neutrophils to remote organs. *J Clin Invest*. 2020; 130: 2301–2318. [PubMed: 31971917]
22. Smith RO, et al. Vascular permeability in retinopathy is regulated by VEGFR2 Y949 signaling to VE-cadherin. *Elife*. 2020; 9
23. Arif N, et al. PECAM-1 supports leukocyte diapedesis by tension-dependent dephosphorylation of VE-cadherin. *EMBO J*. 2021; 40 e106113 [PubMed: 33604918]
24. Nawroth R, et al. VE-PTP and VE-cadherin ectodomains interact to facilitate regulation of phosphorylation and cell contacts. *EMBO J*. 2002; 21: 4885–4895. [PubMed: 12234928]
25. Grazia Lampugnani M, et al. Contact inhibition of VEGF-induced proliferation requires vascular endothelial cadherin, beta-catenin, and the phosphatase DEP-1/CD148. *J Cell Biol*. 2003; 161: 793–804. [PubMed: 12771128]
26. Juettner VV, et al. VE-PTP stabilizes VE-cadherin junctions and the endothelial barrier via a phosphatase-independent mechanism. *J Cell Biol*. 2019; 218: 1725–1742. [PubMed: 30948425]
27. Reynolds AB, et al. SRChing for the substrates of Src. *Oncogene*. 2014; 33: 4537–4547. [PubMed: 24121272]
28. Schimmel L, et al. c-Src controls stability of sprouting blood vessels in the developing retina independently of cell-cell adhesion through focal adhesion assembly. *Development*. 2020; 147
29. Werdich XQ, Penn JS. Src, Fyn and Yes play differential roles in VEGF-mediated endothelial cell events. *Angiogenesis*. 2005; 8: 315–326. [PubMed: 16400523]

30. Eliceiri BP, et al. Selective requirement for Src kinases during VEGF-induced angiogenesis and vascular permeability. *Mol Cell*. 1999; 4: 915–924. [PubMed: 10635317]
31. Bernabeu MO, et al. PolNet: A Tool to Quantify Network-Level Cell Polarity and Blood Flow in Vascular Remodeling. *Biophys J*. 2018; 114: 2052–2058. [PubMed: 29742399]
32. Caolo V, et al. Shear Stress and VE-Cadherin. *Arterioscler Thromb Vasc Biol*. 2018; 38: 2174–2183. [PubMed: 29930007]
33. Wang Y, et al. Ephrin-B2 controls VEGF-induced angiogenesis and lymphangiogenesis. *Nature*. 2010; 465: 483–486. [PubMed: 20445537]
34. Drexler HCA, et al. Vascular Endothelial Receptor Tyrosine Phosphatase: Identification of Novel Substrates Related to Junctions and a Ternary Complex with EPHB4 and TIE2. *Mol Cell Proteomics*. 2019; 18: 2058–2077. [PubMed: 31427368]
35. Friedl P, Mayor R. Tuning Collective Cell Migration by Cell-Cell Junction Regulation. *Cold Spring Harb Perspect Biol*. 2017; 9
36. Lee HW, et al. Role of Venous Endothelial Cells in Developmental and Pathologic Angiogenesis. *Circulation*. 2021; 144: 1308–1322. [PubMed: 34474596]
37. Fernandez-Chacon M, et al. iSuRe-Cre is a genetic tool to reliably induce and report Cre-dependent genetic modifications. *Nat Commun*. 2019; 10: 2262. [PubMed: 31118412]
38. Barbacena P, et al. Competition for endothelial cell polarity drives vascular morphogenesis. *bioRxiv*. 2021. 2021.2011.2023.469704
39. Waschke J, Burger S, Curry FR, Drenckhahn D, Adamson RH. Activation of Rac-1 and Cdc42 stabilizes the microvascular endothelial barrier. *Histochem Cell Biol*. 2006; 125: 397–406. [PubMed: 16195887]
40. Amado-Azevedo J, et al. A CDC42-centered signaling unit is a dominant positive regulator of endothelial integrity. *Sci Rep*. 2017; 7 10132 [PubMed: 28860633]
41. Cao J, Schnittler H. Putting VE-cadherin into JAIL for junction remodeling. *J Cell Sci*. 2019; 132
42. Thurston G, Baldwin AL, Wilson LM. Changes in endothelial actin cytoskeleton at leakage sites in the rat mesenteric microvasculature. *Am J Physiol*. 1995; 268: H316–329. [PubMed: 7840278]
43. Efimova N, Svitkina TM. Branched actin networks push against each other at adherens junctions to maintain cell-cell adhesion. *J Cell Biol*. 2018; 217: 1827–1845. [PubMed: 29507127]
44. Levinson AD, Oppermann H, Levintow L, Varmus HE, Bishop JM. Evidence that the transforming gene of avian sarcoma virus encodes a protein kinase associated with a phosphoprotein. *Cell*. 1978; 15: 561–572. [PubMed: 214242]
45. Erikson RL, Collett MS, Erikson E, Purchio AF. Evidence that the avian sarcoma virus transforming gene product is a cyclic AMP-independent protein kinase. *Proc Natl Acad Sci U S A*. 1979; 76: 6260–6264. [PubMed: 230504]
46. Rohrschneider LR. Adhesion plaques of Rous sarcoma virus-transformed cells contain the src gene product. *Proc Natl Acad Sci U S A*. 1980; 77: 3514–3518. [PubMed: 6251464]
47. Azarnia R, Reddy S, Kmiecik TE, Shalloway D, Loewenstein WR. The cellular src gene product regulates junctional cell-to-cell communication. *Science*. 1988; 239: 398–401. [PubMed: 2447651]
48. Ferrando IM, et al. Identification of targets of c-Src tyrosine kinase by chemical complementation and phosphoproteomics. *Mol Cell Proteomics*. 2012; 11: 355–369. [PubMed: 22499769]
49. Steed E, Rodrigues NT, Balda MS, Matter K. Identification of MarvelD3 as a tight junction-associated transmembrane protein of the occludin family. *BMC Cell Biol*. 2009; 10: 95. [PubMed: 20028514]
50. Martin NG, McAndrew PC, Eve PD, Garrett MD. Phosphorylation of cyclin dependent kinase 4 on tyrosine 17 is mediated by Src family kinases. *FEBS J*. 2008; 275: 3099–3109. [PubMed: 18479465]
51. Lee SW, et al. CD46 is phosphorylated at tyrosine 354 upon infection of epithelial cells by *Neisseria gonorrhoeae*. *J Cell Biol*. 2002; 156: 951–957. [PubMed: 11901164]
52. Varrin-Doyer M, et al. Phosphorylation of collapsin response mediator protein 2 on Tyr-479 regulates CXCL12-induced T lymphocyte migration. *J Biol Chem*. 2009; 284: 13265–13276. [PubMed: 19276087]

53. Takeda H, et al. Comparative analysis of human SRC-family kinase substrate specificity in vitro. *J Proteome Res.* 2010; 9: 5982–5993. [PubMed: 20863140]
54. Tabula Muris C, et al. Single-cell transcriptomics of 20 mouse organs creates a Tabula Muris. *Nature.* 2018; 562: 367–372. [PubMed: 30283141]
55. Frye M, et al. Interfering with VE-PTP stabilizes endothelial junctions in vivo via Tie-2 in the absence of VE-cadherin. *J Exp Med.* 2015; 212: 2267–2287. [PubMed: 26642851]
56. Richards M, et al. Intra-vessel heterogeneity establishes enhanced sites of macromolecular leakage downstream of laminin alpha5. *Cell Rep.* 2021; 35 109268 [PubMed: 34161758]
57. Schmidt TT, et al. Conditional deletion of FAK in mice endothelium disrupts lung vascular barrier function due to destabilization of RhoA and Rac1 activities. *Am J Physiol Lung Cell Mol Physiol.* 2013; 305: L291–300. [PubMed: 23771883]
58. Chen XL, et al. VEGF-induced vascular permeability is mediated by FAK. *Dev Cell.* 2012; 22: 146–157. [PubMed: 22264731]
59. Kasahara K, et al. Rapid trafficking of c-Src, a non-palmitoylated Src-family kinase, between the plasma membrane and late endosomes/lysosomes. *Exp Cell Res.* 2007; 313: 2651–2666. [PubMed: 17537435]
60. Sato I, et al. Differential trafficking of Src, Lyn, Yes and Fyn is specified by the state of palmitoylation in the SH4 domain. *J Cell Sci.* 2009; 122: 965–975. [PubMed: 19258394]
61. Hatanaka K, Simons M, Murakami M. Phosphorylation of VE-cadherin controls endothelial phenotypes via p120-catenin coupling and Rac1 activation. *Am J Physiol Heart Circ Physiol.* 2011; 300: H162–172. [PubMed: 21037229]
62. Grimsley-Myers CM, et al. VE-cadherin endocytosis controls vascular integrity and patterning during development. *J Cell Biol.* 2020; 219
63. Neto F, et al. YAP and TAZ regulate adherens junction dynamics and endothelial cell distribution during vascular development. *Elife.* 2018; 7
64. Nanes BA, et al. p120-catenin regulates VE-cadherin endocytosis and degradation induced by the Kaposi sarcoma-associated ubiquitin ligase K5. *Mol Biol Cell.* 2017; 28: 30–40. [PubMed: 27798235]
65. Dejana E, Orsenigo F. Endothelial adherens junctions at a glance. *J Cell Sci.* 2013; 126: 2545–2549. [PubMed: 23781019]
66. Zarkada G, et al. Specialized endothelial tip cells guide neuroretina vascularization and blood-retina-barrier formation. *Dev Cell.* 2021; 56: 2237–2251. e2236 [PubMed: 34273276]

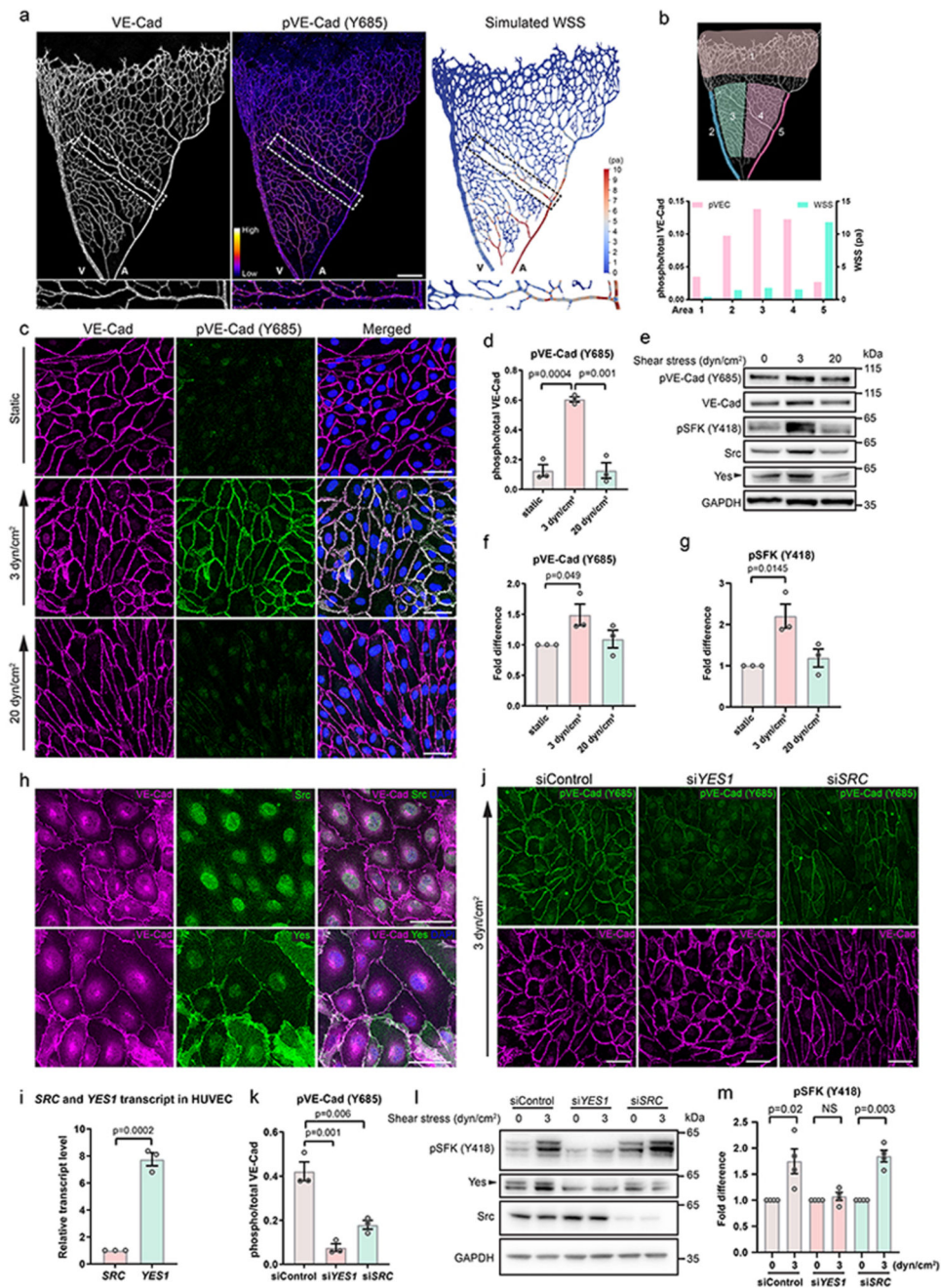


Figure 1. Low shear stress-induced Yes activation

(a) Whole-mount staining of VE-cadherin (left) and pY685 VE-cadherin (middle) and computer-simulated wall shear stress (WSS; right) modelling in the mouse P6 retina. An arterial branch (boxed) is shown in the enlarged pictures below. A, artery; V, vein. Scale bar, 200 μ m. (b) Segmentation of the retina into five regions (upper) and plot (lower) of regional WSS levels (right Y-axis; green bars) and corresponding pY685 VE-cadherin levels (left Y-axis; pink bars) in the different regions. (c) Immunostaining of VE-cadherin (magenta) and pY685 VE-cadherin (green) in HUVECs cultured in static, 3 dyn/cm² and 20 dyn/cm²

conditions for 24 h. Scale bars, 50 μm . **(d)** Ratio of integrated intensity of pVE-cadherin/total VE-cadherin; n=3 independent experiments. **(e)** Representative immunoblot of pY685 VE-cadherin, total VE-cadherin, pY418 SFK, Src, Yes and GAPDH (for normalization) in static or shear stress-treated HUVECs; n=3 independent experiments. **(f, g)** Ratios of pY685 VE-cadherin/total VE-cadherin and pY418 SFK/GAPDH normalized to static conditions, n=3 independent experiments. **(h)** Immunofluorescent staining to show localization of Src and Yes (green) in HUVECs; co-staining of VE-cadherin (magenta). Scale bars, 50 μm . **(i)** Relative expression levels of *SRC* and *YES1* in HUVECs by qPCR. Comparison based on standard qPCR curves for Src and Yes transcripts from 10^{-2} , 10^{-1} , 1, 10, and 100 ng RNA. n=3 independent experiments. **(j)** Immunofluorescence showing pY685 VE-cadherin (green) and total VE-cadherin (magenta) in HUVECs transfected with control, *YES1* or *SRC* siRNA followed by exposure to 3 dyn/cm^2 shear stress for 24 h. Scale bars, 50 μm . **(k)** Quantification of pY685 VE-cadherin integrated intensity normalized to total VE-cadherin. n=3 independent experiments. **(l)** Representative immunoblots of pY418 SFK, Yes and Src in static or shear stress (3 dyn/cm^2) treated control, *YES1* or *SRC* silenced HUVECs; n=4 independent experiments. Quantifications of pY418 SFK normalized to GAPDH in different conditions are shown in **(m)**, n=4 independent experiments. Bar graphs show mean \pm SEM; two-tailed Student's t-test.

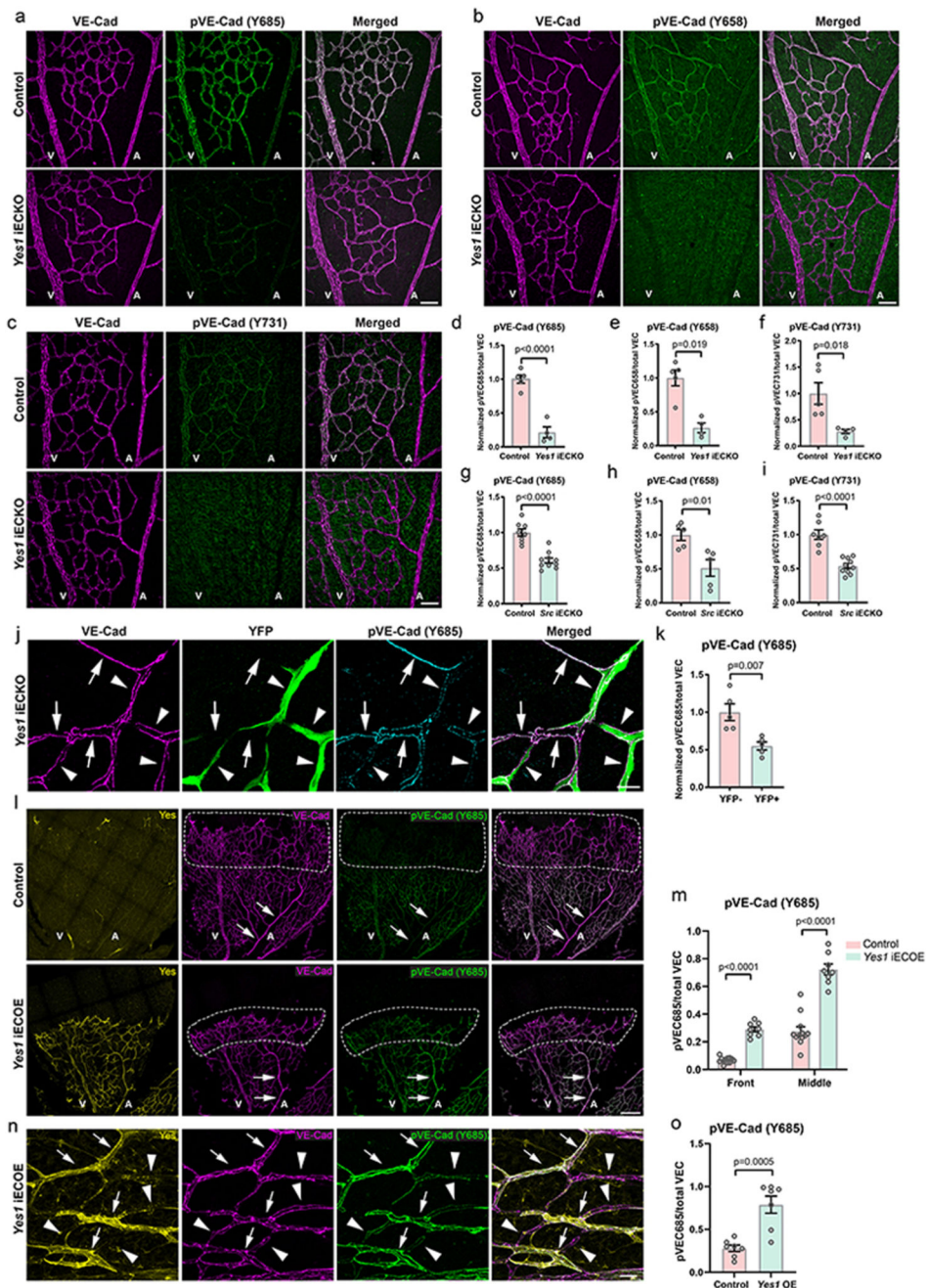


Figure 2. Yes phosphorylates VE-cadherin

(a-c) Immunofluorescence of *Yes1* iECKO (*Yes1* *fl/fl*, *Cdh5CreER*^{T2+}) and control (*Yes1* *fl/fl*, *Cdh5CreER*^{T2-}) P6 retinas showing total VE-cadherin (magenta) and phosphorylated VE-cadherin (green): pY685 (a), pY658 (b) and pY731 (c). Scale bars, 50 μ m. (d-f) Quantification of pVE-cadherin (Y685) (d), pVE-cadherin (658) (e) and pVE-cadherin (731) (f) levels normalized to total VE-cadherin in control and *Yes1* iECKO littermate P6 retinas. Control, n=5; *Yes1* iECKO, n=4. (g-i) Quantification of pVE-cadherin levels normalized to total VE-cadherin in P6 retinas of *Src* iECKO (*Src* *fl/fl*, *Cdh5CreER*^{T2+})

and control (*Src fl/fl, Cdh5CreER^{T2}-*) mice. **(g)** pVE-cadherin (Y685). Control, n=8; *Src* iECKO, n=10. **(h)** pVE-cadherin (Y658). Control, n=5; *Src* iECKO, n=5. **(i)** pVE-cadherin (731). Control, n=7; *Src* iECKO, n=10. **(j)** Immunofluorescence showing the correlation between levels of pY685 VE-cadherin and YFP+ *Yes1*-deficient ECs in a P6 retina with chimeric recombination (100 µg tamoxifen/mouse) at P3. Arrows, YFP-ECs; arrowheads, YFP+ ECs. Scale bar, 20 µm. **(k)** Quantification of pY685 VE-cadherin levels in YFP- and YFP+ ECs. n=5 mice. **(l)** Immunofluorescent images showing *Yes* (yellow), VE-cadherin (magenta) and pY685 VE-cadherin (green) in control (*H11-STOP-Yes1-, Cdh5CreER^{T2}+;* upper panel) and inducible *Yes1* overexpression model (iECO; lower panel) retinas at P6. Arrows indicate arteries. Dashed lines indicate sprouting front. Scale bar, 200 µm. **(m)** Quantification of pY685 VE-cadherin in the front and middle parts of control and *Yes1* iECO retinas. Control, n=12; *Yes1* iECO, n=8. **(n)** Immunofluorescent staining of pY685 VE-cadherin in *Yes1*-overexpressing ECs in a P6 *Yes1* iECO retina with chimeric recombination. Arrows indicate ECs with *Yes1* overexpression, and arrowheads indicate ECs without recombination. Scale bar, 20 µm. **(o)** Quantification of pY685 VE-cadherin in *Yes1*-overexpressing ECs and their neighboring non-recombined ECs, as shown in **(n)**, n=7 mice. V, vein; A, artery. Bar graphs show mean ± SEM; two-tailed Student's t-test.

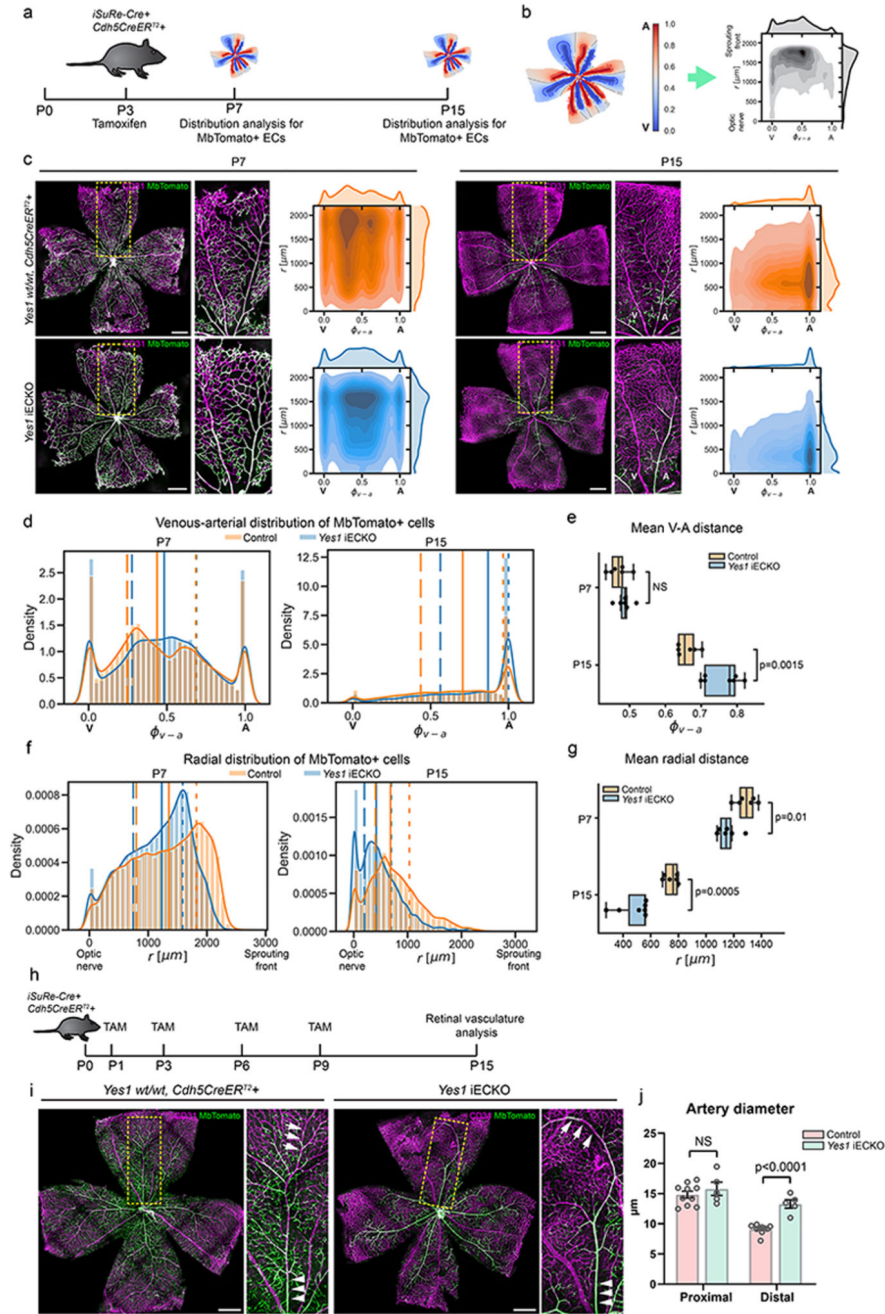


Figure 3. Disturbed collective EC migration in Yes1 deficiency

(a) Timeline for EC distribution analysis (100 μg tamoxifen/mouse at P3). (b) Schematics showing 2D maps of fluorescently labeled ECs in flat-mounted retinas. X-axis; relative distance between veins (0.0) and arteries (1.0), y-axis; distance (μm) from optic nerve to sprouting front. (c) Distribution analysis of ECs with *Cdh5Cre*-induced expression of MbTomato (green) in *Yes1 wt/wt, iSuRe-Cre+, Cdh5CreER^{T2}+*, and *Yes1 fl/fl, iSuRe-Cre+, Cdh5CreER^{T2}+*, at P7 (left) and P15 (right). CD31 (magenta) counterstaining shows all ECs. Boxed regions with veins and arteries shown enlarged (center). Distribution analysis

(right) showing control (orange) and *Yes1* iECKO (blue) ECs. Color density indicates average density of MbTomato+ cells in 6 retinas. V, vein; A, artery. Scale bars, 500 μm . **(d)** Histogram plots of vein-to-artery distribution of MbTomato+ ECs in P7 and P15 retinas. Solid lines indicate median position of total MbTomato+ ECs detected. Dashed lines indicate positions of 25% and 75% of total MbTomato+ ECs. **(e)** Box plot showing mean values of relative vein-to-artery distance of all MbTomato+ ECs/retina. Minima, maxima and center bounds show 25, 75 and 50 percentiles; whiskers show minimum and maximum values. $n=7$ retinas for P15 *Yes1* iECKO, $n=6$ for all other groups; two-sided Welch's t-test. **(f)** Histogram plots showing radial distribution of MbTomato+ ECs in P7 and P15 retinas. Solid lines indicate median position of total MbTomato+ ECs detected. Dashed lines indicate positions of 25% and 75% of total MbTomato+ ECs. **(g)** Box plot showing mean values of radial distance from optic nerve of all MbTomato+ ECs /retina. $n=7$ retinas for P15 *Yes1* iECKO, $n=6$ for all other groups. Minima, maxima, center bounds and whiskers definitions and statistical analyses as in **e**. **(h)** Timeline showing repeated tamoxifen administration. **(i)** P15 retinas from *Yes1* *wt/wt*, *iSuRe-Cre+*, *Cdh5CreER^{T2}+*, and *Yes1 fl/fl*, *iSuRe-Cre+*, *Cdh5CreER^{T2}+* littermates showing *Cdh5*Cre-induced expression of MbTomato+, *Yes1*-deficient ECs (green); counterstaining for CD31 (magenta). Scale bars, 500 μm . **(j)** Average artery diameter in proximal and distal positions (relative to optical nerve) in P15 retinas as shown in **(i)**. Control, $n=10$ retinas; *Yes1* iECKO, $n=5$ retinas. Bar graphs show mean \pm SEM; two-tailed Student's t-test.

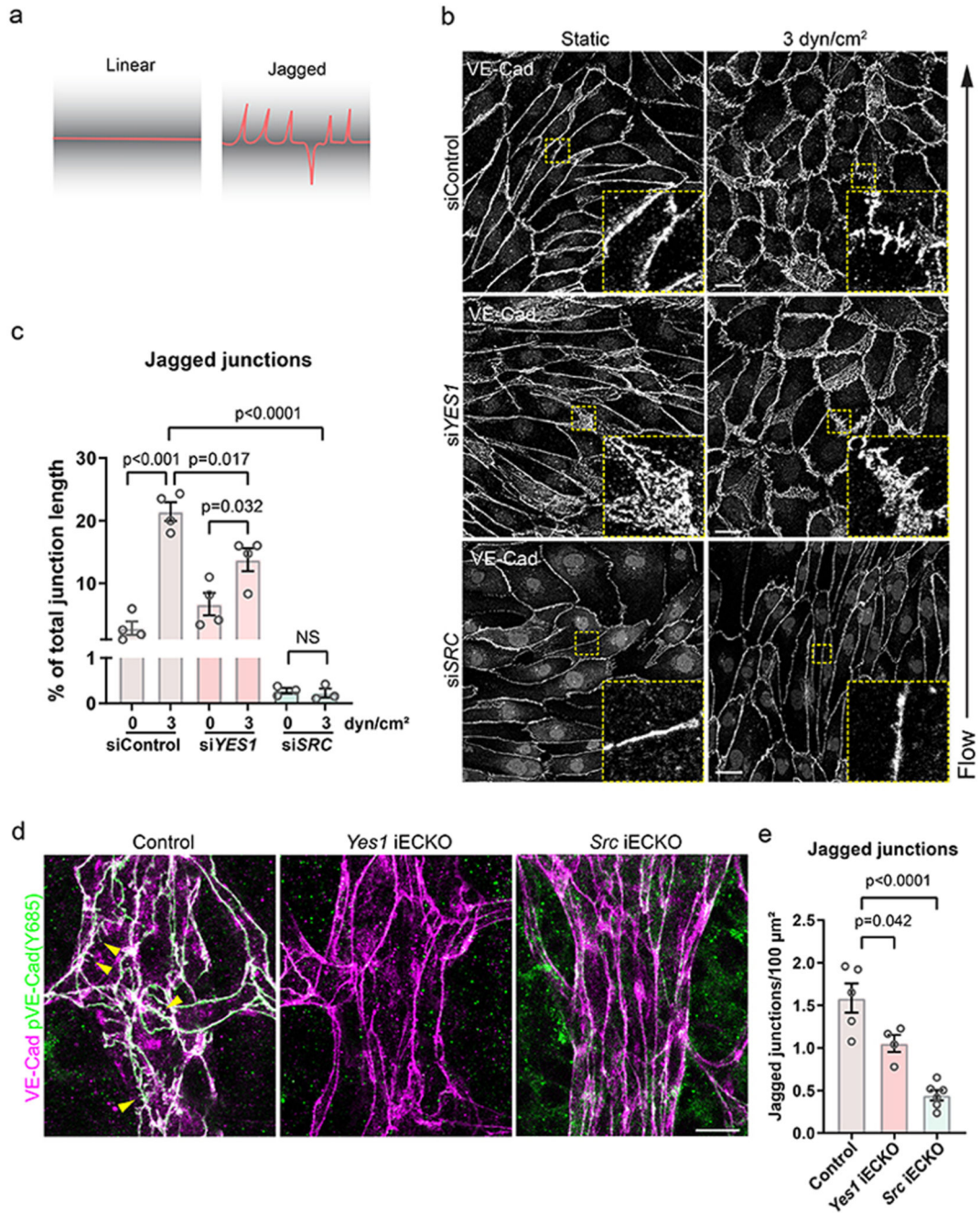


Figure 4. Adherens junction morphology

(a) Schematic outline of linear and jagged adherens junction morphology based on VE-cadherin immunostaining. (b) Immunostaining of VE-cadherin in HUVECs transfected with control or *YES1* or *SRC* siRNA and cultured under static or 3 dyn/cm² flow conditions. Boxed regions show representatives of altered VE-cadherin morphologies, magnified to the lower right. Scale bars, 20 µm. (c) Quantification of jagged junctions as shown in (b), given as junction length in % of total. Bar graphs show mean ± SEM with individual data points. siControl; n=4, si*YES1*; n=4, si*SRC*; n=3 independent experiments. (d) Adherens junction

morphology in veins of retinal vessels at P6 illustrated by immunostaining of VE-cadherin (magenta) and pY685 VE-cadherin (green). Yellow arrowheads indicate jagged junctions. Scale bar, 10 μm . (e) Quantification of jagged structures/100 μm^2 VE-cadherin area in control (*Yes1 fl/fl, Cdh5CreER^{T2}-*), *Yes1* iECKO and *Src* iECKO mouse retinas. Control; n=5 mice, *Yes1* iECKO; n=4 mice, *Src* iECKO; n=6 mice. Bar graphs show mean \pm SEM; two-tailed Student's t-test.

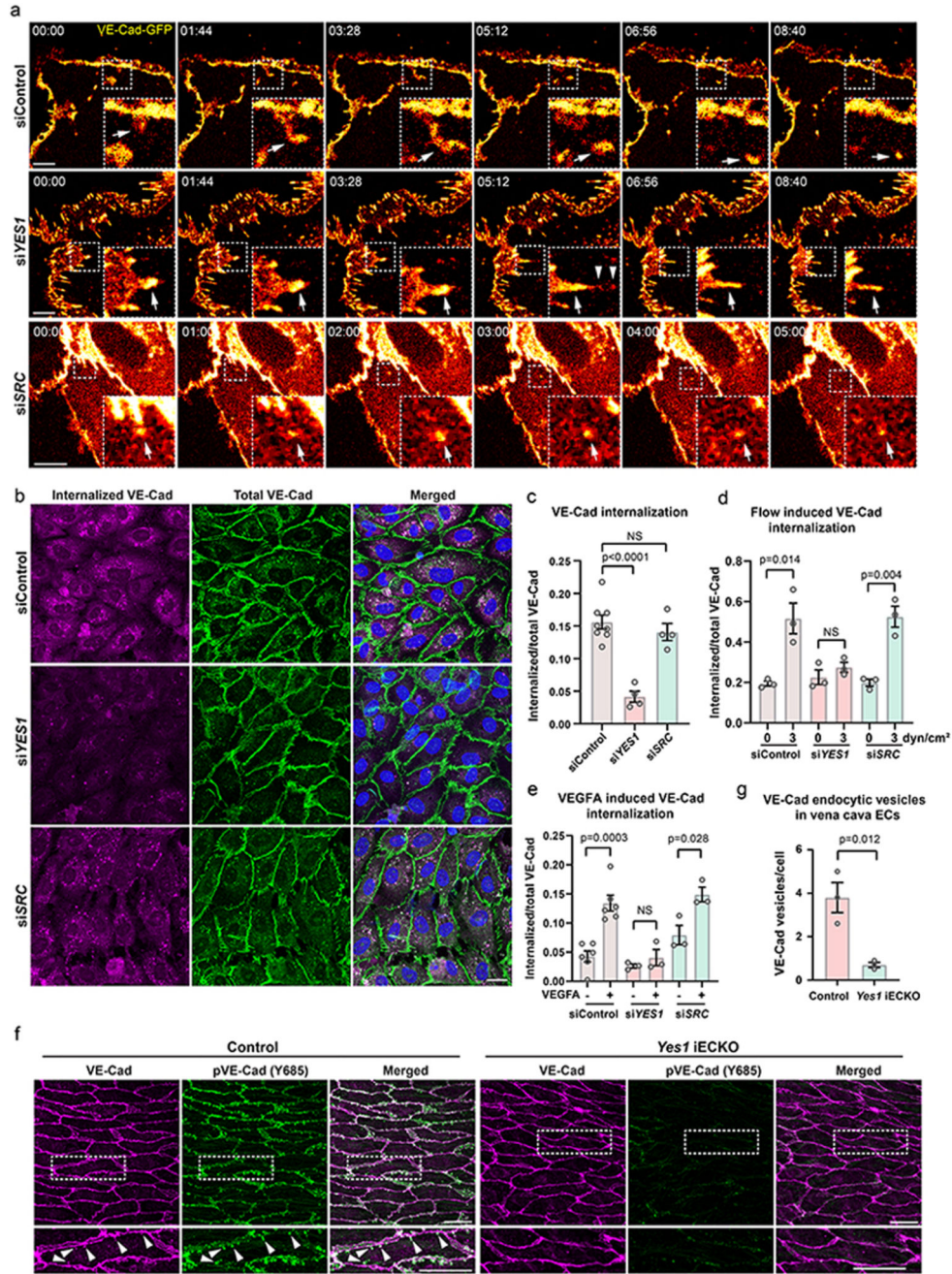


Figure 5. Yes is required for VE-cadherin internalization

(a) Static images from live imaging time series of HUVECs expressing GFP-tagged VE-cadherin. Boxed areas highlight examples of different dynamics of VE-cadherin and are shown enlarged in the lower right. Arrows in the upper (siControl) and lower (siSRC) panel indicate internalized VE-cadherin vesicles. Arrows in the middle panel (siYES1) indicate a junctional VE-cadherin cluster, while arrowheads show detachment and internalization of VE-cadherin from the cluster. Timestamps are min:sec. Scale bars, 10 μ m. (b) Antibody feeding assay showing internalized VE-cadherin (magenta) in control, siYES1 and siSRC

HUVECs co-stained with total VE-cadherin (green) and nuclei (blue). Scale bar, 20 μm . (c) Quantification of internalized/total VE-cadherin in control, *siYES1* and *siSRC* static HUVECs. Control; n=8, *siYES1*; n=4, *siSRC*; n=4 independent experiments. (d) Quantification of flow-induced internalized/total VE-cadherin in control, *siYES1* and *siSRC* HUVECs. n=3 independent experiments. Representative images are shown in Extended Data Fig. 12a. (e) Quantification of internalized/total VE-cadherin in control, *siYES1* and *siSRC* HUVECs treated with VEGFA or not for 3 h. n=3 independent experiments. Representative images are shown in Extended Data Fig. 12b. (f) Internalized VE-Cadherin vesicles at the juxtamembrane regions in mouse *vena cava* ECs shown by immunostaining of VE-Cad (magenta) and pY685 VE-Cad (green). Cells highlighted in boxes are shown enlarged below. Arrowheads indicate internalized VE-Cad vesicles. Scale bars, 20 μm . (g) Quantification of internalized VE-Cad vesicles/cells in control and *Yes1* iECKO *vena cava* ECs. n=3 mice for each group. Bar graphs show mean \pm SEM; two-tailed Student's t-test.

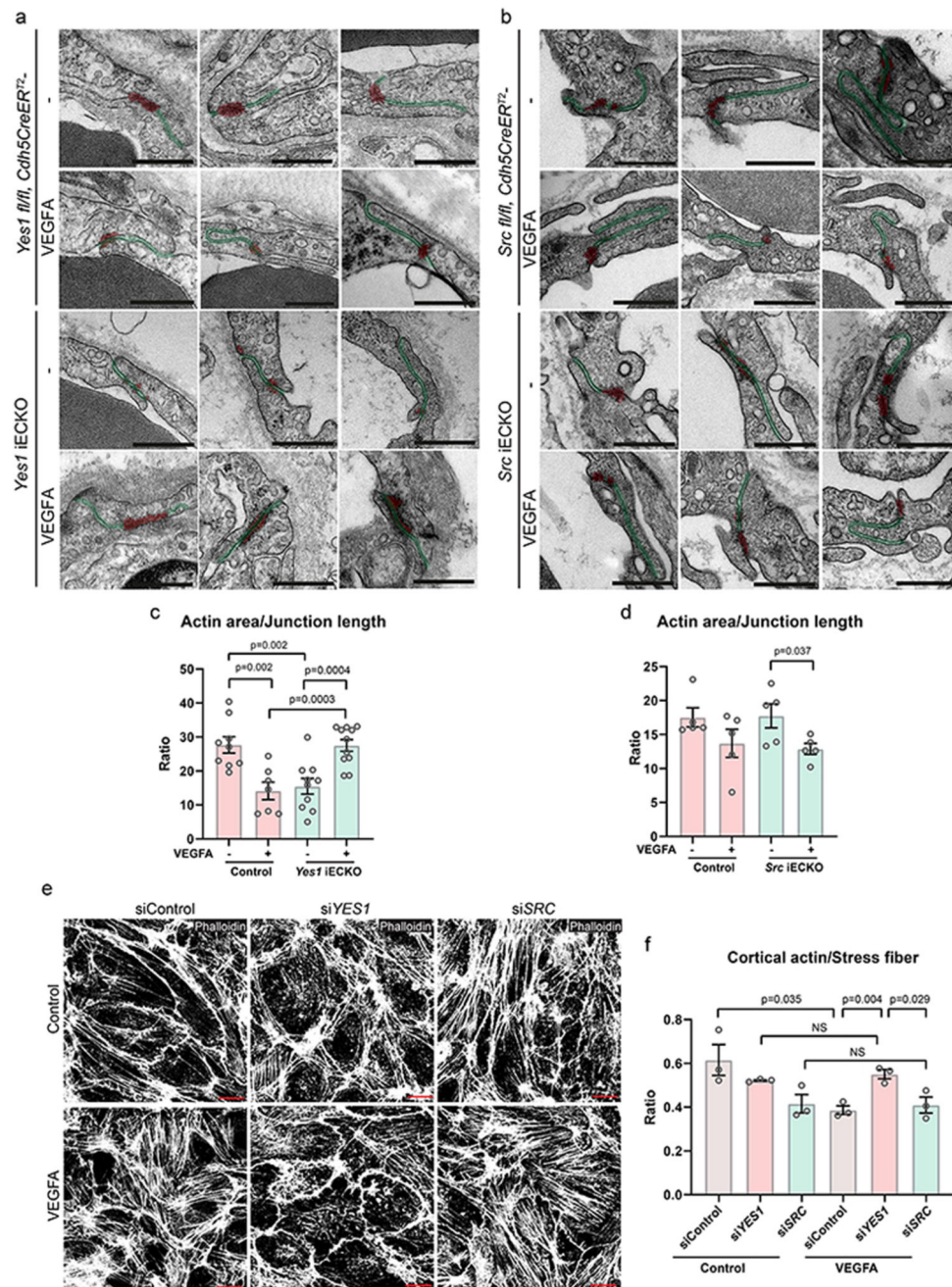


Figure 6. Cell-cell junctions and actin organization

(a, b) Endothelial junctions in control, *Yes1* iECKO or *Src* iECKO mouse ear dermis vessels after intradermal injection of saline or VEGFA164, visualized by transmission electron microscopy. Endothelial cell junction length is highlighted in green, and electron dense junctional area (cortical actin-rich domain) is in red. Scale bars, 500 nm. (c) Quantification of actin area/junction length in control (*Yes1 fl/fl, Cdh5CreER^{T2-/-}*) and *Yes1* iECKO mice. Saline-treated control mice, n=9; VEGFA-treated control mice, n=7; saline-treated *Yes1* iECKO mice, n=10; VEGFA-treated *Yes1* iECKO mice, n=11. 2-40 junctions were analyzed

in each mouse. **(d)** Quantification of electron dense junctional area/junction length in control (*Src fl/fl*, *Cdh5CreER^{T2}-*) and *Src* iECKO mice. n=5 mice for each group. **(e)** Staining with phalloidin shows the arrangement of actin stress fibers and cortical actin in HUVECs treated with control, Yes or Src siRNA followed by VEGFA stimulation for 15 min. Scale bars, 20 μ m. **(f)** Quantification of the integrated intensity of actin stress fibers normalized to cell numbers in control, Yes- or Src-silenced HUVECs. n=3 independent experiments. Bar graphs show mean \pm SEM; two-tailed Student's t-test.

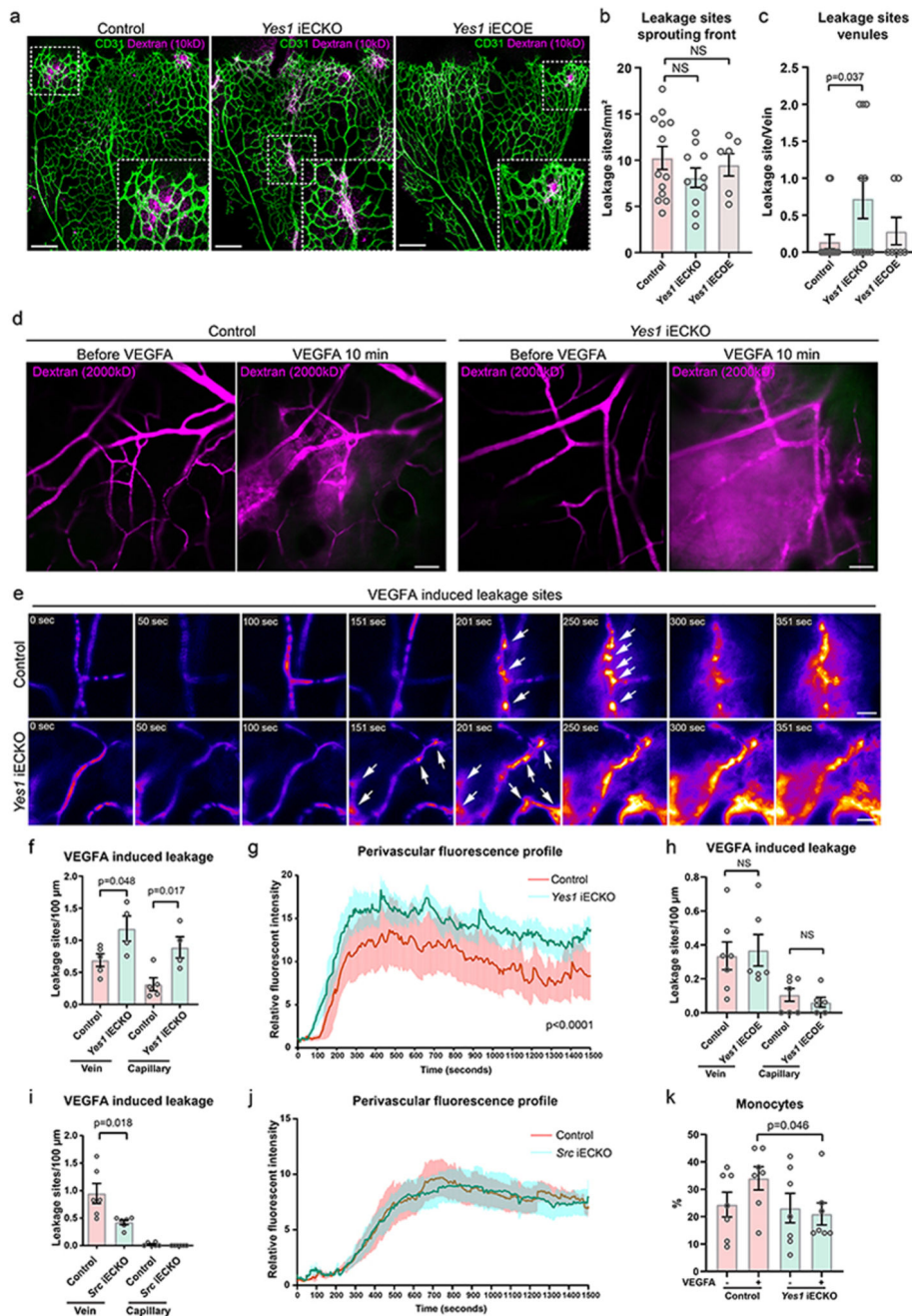


Figure 7. Yes-deficiency leads to loss of vascular integrity

(a) Perivascular leakage of 10 kD dextran (magenta) in fixed P6 retinas of control (*Yes1 fl/fl, Cdh5CreER^{T2}-*), *Yes1* iECKO and *Yes1* iECO mice. Vessels shown by CD31 immunostaining (green). Boxed leakage sites shown in magnification. Scale bars, 200 μ m. (b) Quantification of leakage sites at the sprouting front. Control, n=9 retinas; *Yes1* iECKO, n=10 retinas; *Yes1* iECO, n=6 retinas, two-tailed Student's t-test. (c) Quantification of leakage sites in retinal veins. Control, n=14 veins/ 9 retinas; *Yes1* iECKO, n=11 veins/10 retinas; *Yes1* iECO, n=7 veins/ 6 retinas; two-tailed Student's t-test. (d) Static images

from intravital time series imaging of mouse ear dermal vessels before and 10 min after intradermal VEGFA injection. Leakage visualized by the perivascular accumulation of 2000 kDa dextran (magenta). Scale bars, 50 μm . (e) Heat map images of individual leakage sites (arrows) after VEGFA injection. Scale bars, 20 μm . (f) Quantification of individual leakage sites at veins and capillaries in control and *Yes1* iECKO mice induced by VEGFA. Control, n=5 mice, *Yes1* iECKO, n=4 mice. (g) VEGFA-induced changes in perivascular fluorescence intensity measured at 2-second intervals for 1500 seconds. Curves show mean values of 8 leakage sites from 5 control mice and 10 sites from 4 *Yes1* iECKO mice; two-way ANOVA. (h) Quantification of individual leakage sites at veins and capillaries of control (*H11-STOP-Yes1⁻, Cdh5CreER^{T2+}*) and *Yes1* iECOIE mice induced by VEGFA. Control, n=7 mice, *Yes1* iECOIE, n=6 mice. (i) Quantification of individual leakage sites at veins and capillaries in the ear dermis of control (*Src fl/fl, Cdh5CreER^{T2-}*) and *Src* iECKO mice after VEGFA injection. Control, n=6 mice, *Src* iECKO, n=6 mice. (j) VEGFA-induced changes in perivascular fluorescence intensity measured at 2-second intervals for 1500 seconds. Control, n=6 mice, *Src* iECOIE, n=6 mice; two-way ANOVA. (k) FACS analysis of monocyte/macrophage (CD11b⁺, LY6G⁻) extravasation in peritoneal fluid from control and *Yes1* iECKO mice 24 h after i.p. injection with saline or VEGFA, n=7 mice for each group. Bar graphs show mean \pm SEM; two-tailed Student's t-test.

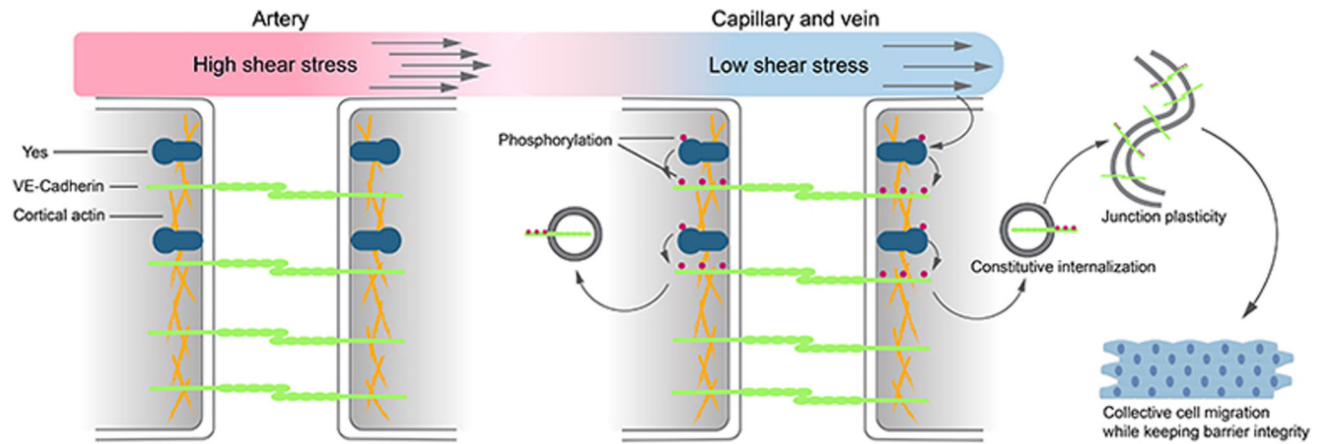


Figure 8. Low flow-induced *Yes* kinase activity controls EC junctions

Yes protein-tyrosine kinase is inactive under the high shear stress in arteries. Low shear stress level in capillaries and veins activate Yes kinase activity, which phosphorylates the adherens junction protein VE-cadherin at Y658, Y685 and Y731. Phosphorylation of VE-cadherin is required for its constitutive internalization which confers EC junctional plasticity. Junctional plasticity is essential for collective EC migration during angiogenesis as well as for maintaining vascular barrier integrity.